

Bioinspired microneedle patches: biomimetic designs, fabrication and biomedical applications

Pooyan Makvandi^{*†1}, Aziz Maleki^{‡2}, Majid Shabani^{†1,3}, Aaron RJ Hutton⁴, Melissa Kirkby⁴, Rezvan Jamaledin⁵, Tianxu Fang^{6,7}, Jiahuan He⁶, Jesse Lee⁶, Barbara Mazzolai¹, Ryan F Donnelly⁴, Franklin R Tay⁸, Guojun Chen^{6,7,*}, Virgilio Mattoli^{1*}

¹Istituto Italiano di Tecnologia, Centre for Materials Interface, viale Rinaldo Piaggio 34, 56025 Pontedera, Pisa, Italy

²Department of Pharmaceutical Nanotechnology, School of Pharmacy, Zanjan University of Medical Sciences, 56184-45139 Zanjan, Iran

²Zanjan Pharmaceutical Nanotechnology Research Center (ZPNRC) Zanjan University of Medical Sciences Zanjan 45139-56184, Iran

³The BioRobotics Institute, Scuola Superiore Sant'Anna, viale Rinaldo Piaggio 34, 56025 Pontedera, Pisa, Italy

⁴School of Pharmacy, Queen's University Belfast, 97 Lisburn Road, Belfast, BT9 7BL, United Kingdom

⁵ Center for Advanced Biomaterials for Health Care (iit@CRIB), Italian institute of technology, Naples 80125, Italy

⁶The Rosalind & Morris Goodman Cancer Research Institute, McGill University, Montreal, QC H3G 0B1, Canada

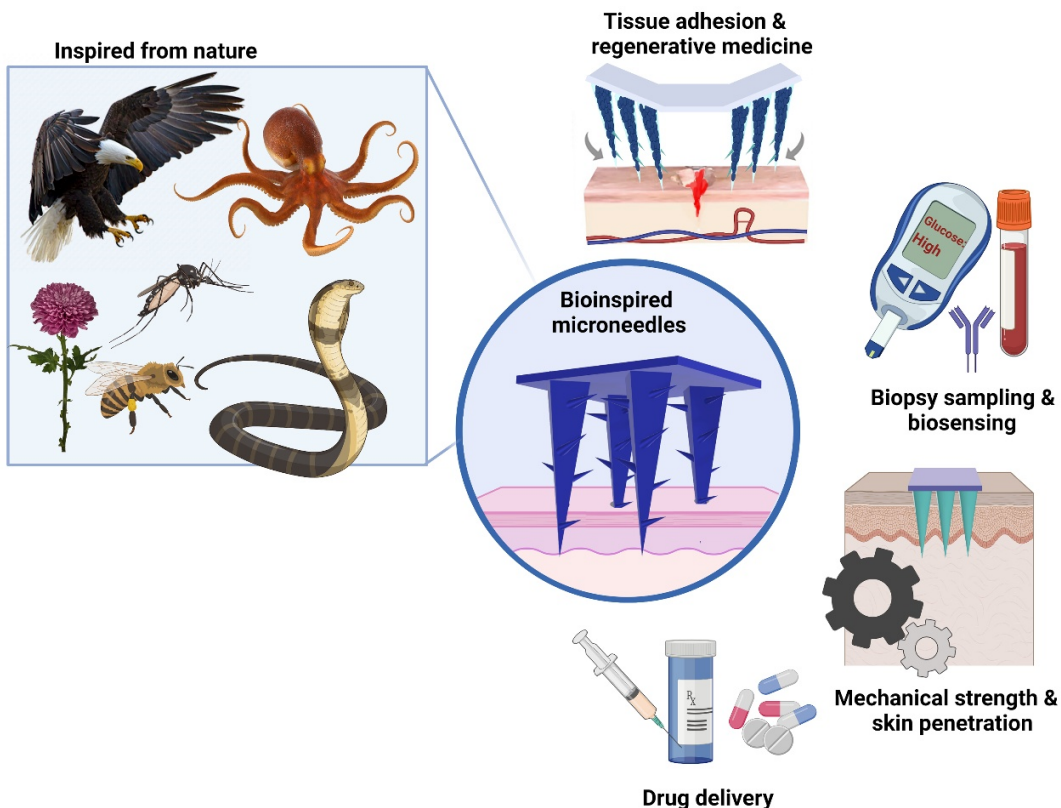
⁷Department of Biomedical Engineering, McGill University, Montreal, QC H3G 0B1, Canada

⁸The Graduate School, Augusta University, Augusta, GA 30912, USA

[†]Equally contributed to this work

***Corresponding authors:**

E-mails: pooyan.makvandi@iit.it (P. M.); guojun.chen@mcgill.ca (G. C.); virgilio.mattoli@iit.it (V. M.)



Summary

Nature contains abundant systems that can significantly alter their structures and properties to adapt to the surrounding environment. Through natural selection and unceasing evolution, hierarchical architectures and sophisticated strategies have been created by nature to achieve optimally adapted materials for biomedical applications. The development of microneedles has advanced to the next generation of bioinspired microneedles, with the goal of improving functions such as amelioration of mechanical properties and tissue adhesion. The biomimetic designs and structures of microneedles are highlighted in the present review. This is followed by an in-depth discussion of the fabrication approaches from molding techniques to 3D and 4D printing. The medical applications of bioinspired microneedles, including drug delivery, regenerative medicine,

biopsy sampling and biosensing, are also discussed. Lastly, future opportunities and challenges with respect to clinical translation are also deliberated.

Keywords: Bioinspired design; biomimetic structures; microneedle patches

Table of Contents

1.	Introduction	5
2.	Bioinspired designs and structures: Why biomimetic?	6
3.	Fabrication of BMNs: From traditional to novel approaches.....	8
3.1	Traditional molding techniques.....	8
3.1.1	MN molding using solvent casting	8
3.1.2	MN molding and polymerization.....	9
3.2	Novel molding techniques.....	12
3.2.1	Ferrofluid configured molding.....	12
3.2.2	Magnetorheological drawing lithography.....	14
3.3	Three-dimensional printing	14
3.3.1	Fused deposition modeling	16
3.3.2	Stereolithography	17
3.3.3	Digital light projection.....	18
3.3.5	Two-photon polymerization.....	21
3.4	Four-dimensional printing.....	23
4.	Bioinspired microneedles: Toward boosting performance and application	26
4.1.	Drug delivery.....	32
4.2.	Wound healing and regenerative medicine	37
4.3.	Biopsy sampling and biosensing	44
4.4.	Optimization of mechanical strength and skin penetration.....	47

5.	Challenges and future perspectives	51
	Acknowledgments.....	53
	References.....	54

Highlights

Design, structure, and performance of nature-inspired microneedles

Fabrication approaches, e.g. molding techniques and 3D and 4D printing methods

Biomedical application of bioinspired microneedle patches

Progress and potential

Nature provides abundant systems that can significantly alter their structures and properties to adapt to the surrounding environment. Over the billions of years of evolution, hierarchical architectures and sophisticated strategies have been created through natural selection to achieve optimally adapted materials with specific functions. In this regard, bioinspired engineering is involved in the design and fabrication of advanced materials in many fields of research and technology. To reach optimal microneedle performance, researchers have developed a newer class of microneedle patches, known as biomimetic or bioinspired microneedles (BMNs) which have a diverse set of applications. The applications of BMNs, including drug delivery, tissue adhesion and regenerative medicine, as well as interstitial fluid extraction are discussed to provide an overall backdrop for future research in this fascinating field of development. These information provide a deeper understanding of the design and application of nature-inspired microneedles to provide a backdrop for future research.

Pros

Depending on the targeted application, nature-inspired microneedles may benefit from the following features:

- Improved adhesion to the underlying tissue

- Improved tissue penetration
- Enhanced drug loading or encapsulation
- Rapid injection of bioactive molecules
- Constructing and maintaining micro-holes on skin

Cons

Depending on the animal- or plant-mimicked structures, nature-inspired microneedles may suffer from the following features when compared with traditional microneedles:

- Complicated design and structure
- Complex architecture for fabrication - an obstacle for scale-up
- Multifaceted construction needs sophisticated equipments

1. Introduction

Microneedles (MNs) are micro-scale needles that are utilized in the biomedical sector for applications such as transdermal drug delivery and tissue engineering.^{1–3} They are used to achieve optimal tissue contact in a minimally-invasive, easy-to-use and painless manner via penetration into the skin without touching blood capillaries and nerve endings.^{4–6}

To achieve optimal microneedle performance, researchers have developed a novel class of microneedle patches that are known as biomimetic or bioinspired microneedles (BMNs). These BMNS have diverse applications.^{7–9} Over the ages, nature has created optimized solutions for many problems through the process of evolution.¹⁰ The fascinating properties observed in various natural species offer excellent opportunities to develop BMNs with functionalities that approximate their natural counterparts. These biomimetic simulations are achieved via manipulation of morphology, structure and chemistry.^{7,8}

Representative examples are used in the present review to highlight how properties originating from living organisms (e.g. teeth of limpets,¹¹ stingers of honeybees,¹² mosquito/endoparasite *Pomphorhynchus laevis*'s proboscis,^{13,14} clawed toes of eagles,⁸ snake fangs⁷) may be exploited with mimicking tactics to design microneedles with specific

functionalities to overcome challenges that are faced by conventional microneedles. Bioinspired designs as well as their structures and medical significance are highlighted. The techniques for fabricating BMNs, ranging from traditional to sophisticated approaches, are introduced. The applications of BMNs, including drug delivery, tissue adhesion and regenerative medicine, as well as interstitial fluid extraction are discussed to provide a backdrop for future research in this fascinating field of development.

2. Bioinspired designs and structures: Why biomimetic?

Nature has evolved continuously since the advent of life on earth around 3.8 billion years ago.¹⁵ Nature has created abundant systems that can significantly change their structures and properties to adapt to the surrounding environment. Over the billions of years of evolution, hierarchical architectures and sophisticated strategies have been created through natural selection to achieve optimally-adapted materials with specific functions. The dimensions of these materials range from the macroscale to the nanoscale.¹⁶ The tactic of mimicking animal and plant organs appears to be a slick-as-whistle strategy for attaining the desired functions. Bioinspired engineering is involved in the design and fabrication of advanced materials in many fields of research and technology. These exciting areas of exploration include energy storage, mechanical materials and biomedical applications.¹⁷ Understanding structure-property relationships in natural materials paves the way to emulate their morphology and functions in the design of bioinspired advanced functional materials.¹⁸ There is a large number of flora and fauna with specific properties that enable researchers to design and produce diverse bioinspired materials.¹⁰ Such characteristics represent gifts from nature to mankind. Examples are plentiful: damage-tolerant materials inspired by the nacre,^{19–21} antifogging coatings inspired by the insect compound eye,²² artificial armors inspired by the fish scale and armadillo shell,²³ strong tissue adhesion inspired by the swellable proboscis of endoparasitic worms,¹⁴ water harvesting inspired by desert beetle and cactus,²⁴ photonic materials inspired by opal, butterfly wings and chameleon,^{25,26} superadhesive materials inspired by the gecko feet and mussels,^{27,28} ultrafast water transport inspired by insect trapping plants,²⁹ self-cleaning surfaces inspired by the lotus leaf and cicada wing,^{30,31} oil–water separation inspired by the fish-gill and cactus-needle,³² construction of lightweight and strong structural materials inspired by the brick-and-mortar-like structure of nacre,³³ as well as micro-hooks

inspired by plants for controlled adhesion and grasping.³⁴ **Figure 1** summarizes the representative applications of BMNs and their inspiration from nature.

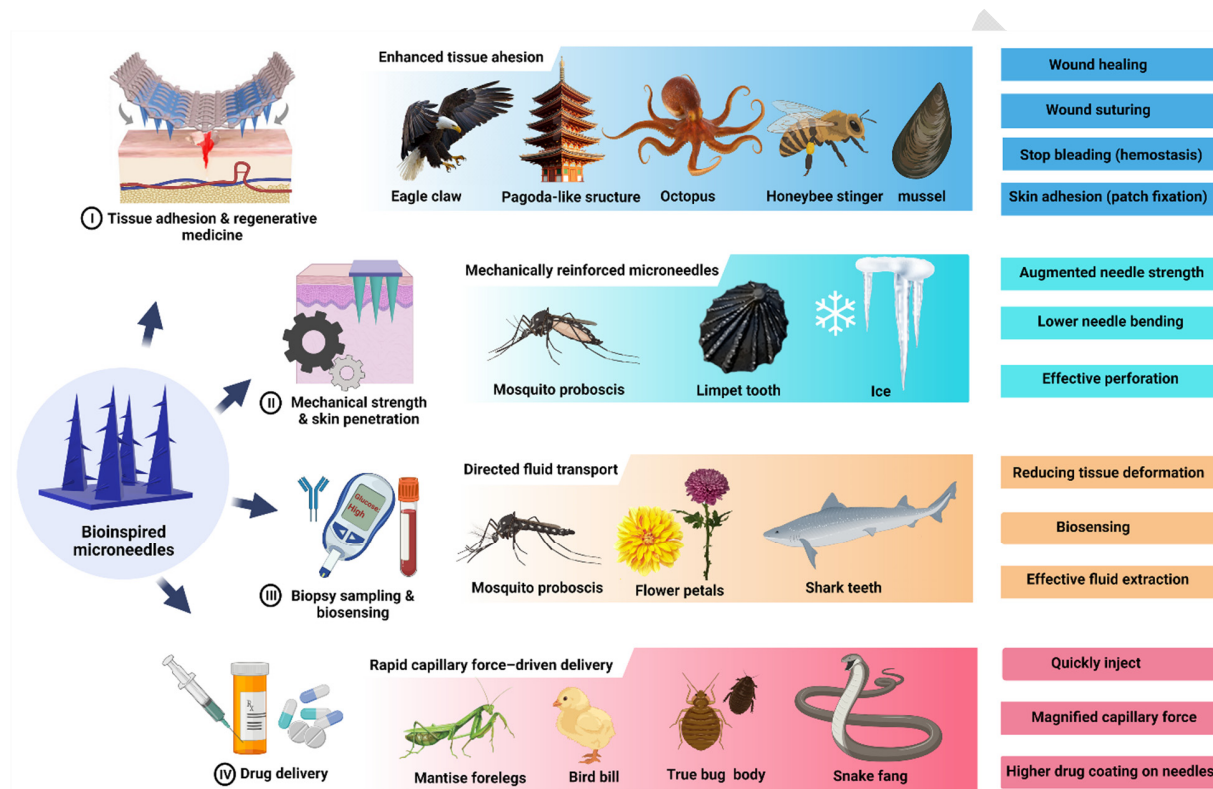


Figure 1: Nature-inspired design. Schematic showing various living creatures and their selected functions that have been exploited in the design and fabrication of BMN patches for diverse biomedical applications.

It is worth noting that in many cases, the desired function is accomplished without changing the chemistry of materials, but rather through materials engineering. For example, the color of butterfly wings and peacock feathers is achieved without using any pigment. This so-called structural color originates from the interaction between light and sophisticated nano-architectures.³⁵ Octopuses have clusters of suckers on their tentacles that enable them to move and catch prey; each sucker contains an orifice and a protuberance. Such an ingenious architectural design allows the soft-bodied animal to adhere to both dry and wet objects through their suction cups and the inner dome-like protuberances. Adhesion strategies found in nature that involve

molecular attractions or mechanical interlocking between surfaces have inspired scientists to design artificial adhesives that retain their adhesiveness in both wet and dry conditions.^{36,37}

Inspired by nature, BMNs are a novel class of microneedles that are engineered to overcome the shortcomings faced by conventional microneedles.^{18,38} Well-evolved microarrayed structures found in nature provide scientists with inspiration for developing novel microneedles with specific functionalities. For instance, sticky BMN patches inspired by the clawed toes of eagles promote incisional wound healing.⁸ Bioinspired microneedles that contain multiple open grooves on their surfaces are inspired by the mono-grooved fangs of rear-fanged snakes that generate a rapid capillary force–driven delivery system.⁷ Likewise, BMN patches with backward-facing curved barbs for enhanced tissue adhesion are enthused by the stinger of honeybees.¹² Painless BMNs designed for blood collection without bleeding are inspired by the proboscis of mosquitoes.¹³ An overview of rationally-designed BMN patches inspired by nature and the importance of BMN patches over conventional microneedles will be detailed in the next section.

3. Fabrication of BMNs: From traditional to novel approaches

3.1 Traditional molding techniques

The use of traditional molding techniques such as drawing lithography and hot embossing to produce BMNs is of considerable challenge. Micromolding using solvent casting appears to be the only time-tested method that is successful in this new era of microneedle design. This technique encompasses a multistep process that typically involves the creation of a female mold using laser engineering. This female mold is typically composed of polydimethylsiloxane (PDMS), a hydrophobic material that possesses excellent thermal stability, good transcription ability, low adhesion and can be easily reproduced.^{39,40} Using PDMS molds, BMNs have been manufactured using solvent casting alone or in combination with polymerization, as discussed below.

3.1.1 MN molding using solvent casting

Inspired by the proboscis of endoparasitic spiny-headed worms (*Pomphorhynchus laevis*), structured biphasic microneedles have been developed using solvent casting (**Figure 2A**).¹⁴ The mechanism of microneedle insertion and tissue retention is based on the adaptable morphology of this worm species. The worm anchors firmly to the soft tissue within its host by expanding into a bulb-like structure via retractor muscles located at the base of the proboscis.⁴¹ To achieve

mechanical interlocking of the microneedle upon skin insertion, solvent casting was used to generate a rigid inner core surrounded by a soft outer region. Firstly, the polystyrene-block-poly(acrylic acid) (PS-*b*-PAA) block copolymer was dissolved in *N*-dimethylformamide prior to casting into PDMS molds. A non-swellable PS homopolymer was melted at 180 °C under vacuum and added on top of the swellable PS-*b*-PAA layer to generate the supporting inner core. This microneedle design exhibited excellent adhesion to soft tissues, with no adverse reactions reported. Using an identical solvent casting method, bullet-shaped biphasic microneedles have been fabricated more recently, with enhanced skin surface adhesion and swelling capability (**Figure 2B**).⁴²

3.1.2 MN molding and polymerization

By mimicking the insertion mechanism of the endoparasite proboscis, another biphasic microneedle device has been developed using molding and polymerization.⁴³ Biocompatible solvents and low temperatures were used during fabrication. An aqueous blend of a mussel adhesive protein (MAP), hyaluronic acid, tris(bipyridine) ruthenium(II) chloride (Ru(II)bpy₃²⁺) and sodium persulfate dissolved in phosphate-buffered saline was cast in PDMS molds and kept under vacuum pressure for a defined time-period. This aqueous blend constituted the swellable outer layer, achieved via a light-activated tyrosine crosslinking system. This well-documented reaction involves the activation of Ru(II)bpy₃²⁺ with sodium persulfate, an electron receptor, in the presence of ultraviolet light.^{44,45} This generates Ru(III) and sulfate radical; the Ru(III) oxidizes tyrosine residues on the MAP and the radical facilitates cross-linking through arene coupling.

The second inner layer was composed of silk fibroin, Ru(II)bpy₃²⁺ and sodium persulfate dissolved in deionized water and subjected to backside vacuum. This microneedle design enabled effective skin insertion and surface adhesion. Skin adhesion was achieved through coacervation between the cationic MAP and anionic hyaluronic acid. Previous studies have shown that MAPs effectively adhere to biological tissues through hydrogen bonding, cation-π interactions, π-π stacking and electrostatic interactions.^{46–48} Because this biocompatible hydrogel-forming microneedle device displayed strong tissue adhesive properties and effective wound regeneration, such a design has potentially important benefits for regenerative closure of both superficial and deep abrasions.⁴³

A BMN was synthesized recently by mimicking the suction cups of octopus tentacles.⁴⁹ A specially designed negative mold was used to create microneedles that consisted of 600 µm long conical needles. Each needle was inspirationally surrounded by 6 suction cups. A solution of poly(ethylene glycol) diacrylate (PEGDA), 2-hydroxy-2-methylpropiophenone (HMPP) and sodium alginate was used to fabricate the microneedle tips. The solution was solidified by ultraviolet-mediated polymerization for 15 sec. The microneedle baseplate was composed of sodium periodate, dopamine hydrochloride and gelatin. The mixture was left at room temperature for 20 min to permit gelation. Polymerization occurred through the Schiff base and Michael addition reactions. Incorporation of sodium periodate resulted in the oxidation of dopamine, causing the latter to cross-link with the gelatin backbone. These microneedle arrays demonstrated excellent adhesive properties especially in highly-mobile body parts. This microneedle design has the potential to deliver a wide range of therapeutic compounds because of the avoidance of harsh solvents, high temperatures and prolonged exposure to ultraviolet light during the manufacturing process.

Another method for polymerization and casting is based on photocurable monomers, such as methacrylated polysaccharides and proteins (e.g. methacrylated-hyaluronic acid and gelatin, respectively). Using this approach, pagoda-like multilayered BMNs have been developed.⁵⁰ This design was inspired by the hierarchical microstructure of feet or stings of insects such as ladybugs, gadflies and wasps. As shown in **Figure 2C**, the first layer of the BMN was made by mold replication. The multilayered design was created by using a hollow heightening pad to repeatedly stack the pre-polymer filling negative mold. Rapid hemostasis was reported by coating this BMN with dodecyl-modified chitosan.⁵⁰ Specifically, physical interlocking of the BMN within tissues enabled strong adherence, even in areas with ample blood loss. This was demonstrated in an *in vivo* rabbit model, in which acute tissue injuries, such as liver bleeding, spleen bleeding and kidney bleeding, ceased immediately following the application of dodecyl-modified chitosan-coated multilayered BMNs. This BMN design may play a potential role in tissue repair and wound management.

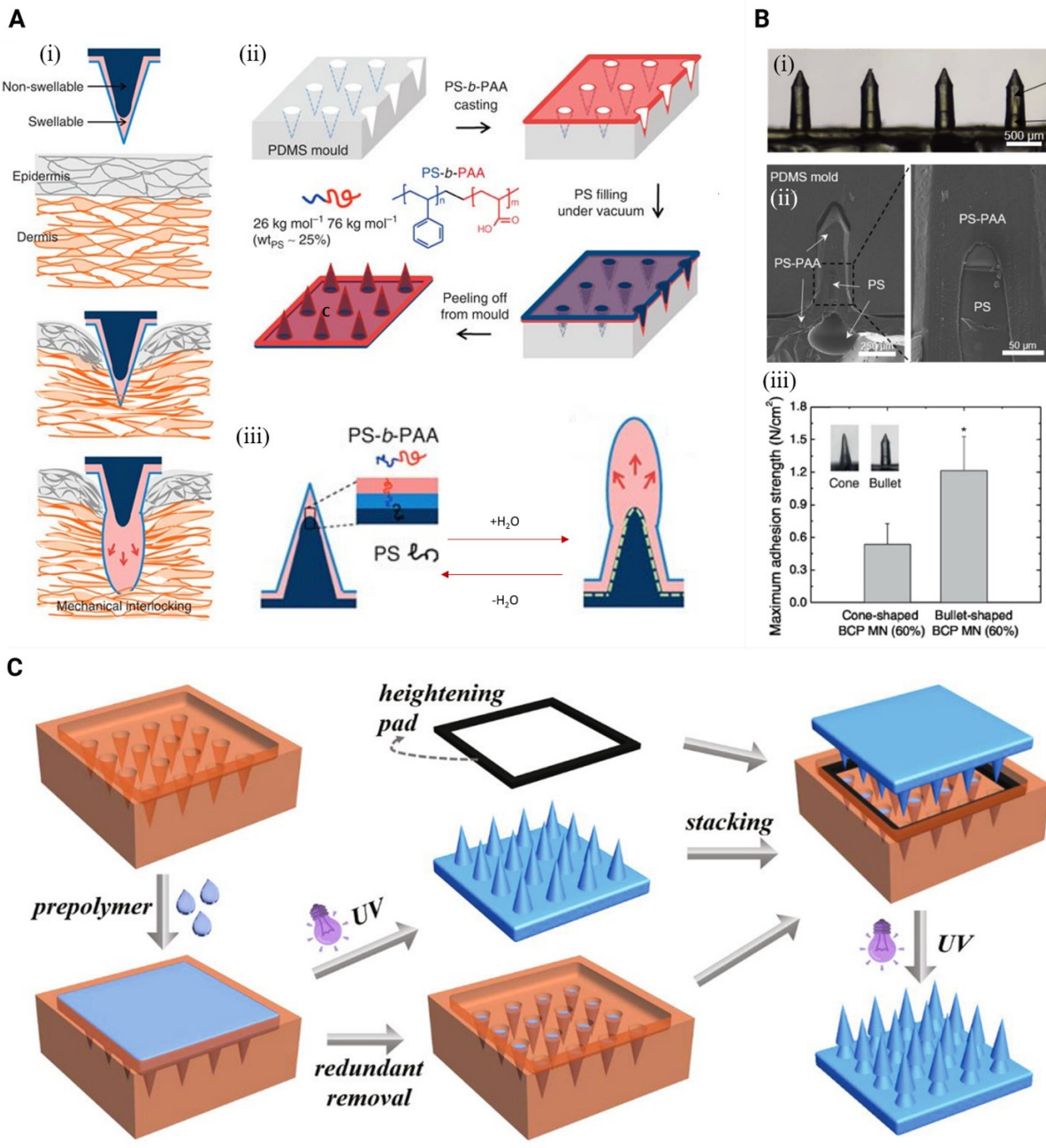


Figure 2 Molding with solvent casting or polymerization. A) (i) Illustration showing the mechanical interlocking mechanism of the biphasic microneedles upon application to the skin tissue. (ii) In the solvent casting technique, polystyrene-block-poly(acrylic acid) (PS-*b*-PAA) was first cast into PDMS molds. This was followed by the addition of melted PS pellets at 180 °C under vacuum pressure. (iii) The double-layered microneedles consists of a swellable outer surface and a non-swelling inner core. The outer surface is capable of reversible bulb formation upon hydration. Reprinted from ¹⁴ with permission from Springer Nature. B) Optical image (i) and SEM image (ii) of bullet-shaped PS-*b*-PAA block copolymer microneedle. (iii) Comparison between the adhesion strength of cone-shaped *vs* bullet-shaped microneedles. Reprinted

from⁴² with permission from Elsevier. (C) Fabrication of bioinspired pagoda-like microneedle patches using a combination of molding and polymerization techniques. Reprinted from⁵⁰ with permission from Elsevier.

3.2 Novel molding techniques

3.2.1 Ferrofluid configured molding

Top-down approaches such as micromolding have shown great promise in the fabrication of BMNs. However, these approaches only produce microneedles that are perpendicularly orientated to the base plate. This ultimately limits the number of bioinspired designs that may be created. Ferrofluid configured molding has recently been developed to overcome this issue.⁵¹ Ferrofluids consist of ferromagnetic nanoparticles which enable magnetically-orientated patterns to be produced under the application of an external magnetic field.⁵² Altering the position of the strong magnetic force enables the actively-tunable ferrofluids to form cone-like spikes.⁵³ Using this approach, a microneedle based on the serrated microstructures present on the forelegs of praying mantises has been developed (**Figure 3A**).⁵¹ In this example, ferrofluid was dispersed in a prepolymer mixture of ethoxylated trimethylolpropane triacrylate (ETPTA), an ultraviolet light-curable agent and 2-hydroxy-2-methylpropiophenone (HMPP), a photoinitiator, in a Petri-dish. Ferrofluid droplets were formed by adjusting the distance between the Petri dish and the magnetic field, ultimately creating an asymmetrical microneedle array. As shown in **Figure 3A**, tilting the magnet enabled the conical droplets to be altered to the required angle, which ranged from 30° to 90°, before solidifying the mixture under ultraviolet light. A serrated clamping hydrogel microneedle array was then fabricated using silk fibroin. This solution was used to coat the outer layer of the needle tips. An ultraviolet light-cured mixture of poly(ethylene glycol) diacrylate (PEGDA) and HMPP was used to generate the inner layer to increase rigidity and to prevent the microneedles from collapsing upon drying. When compared to perpendicular microneedle arrays, these novel microneedle arrays displayed improved adhesion properties in mouse models.⁵¹ However, there must be a fine balance between the adhesion strength and the ease of removal. If adhesion is too strong, there is the possibility that these microneedle patches become painful upon removal. In addition, the relatively complex nature of this fabrication process may limit the applications of these BMNs. That said, serrated clamping hydrogel microneedle arrays are undoubtedly an interesting concept and have potential for improving microneedle insertion and adhesion, which are important considerations for their practical use.

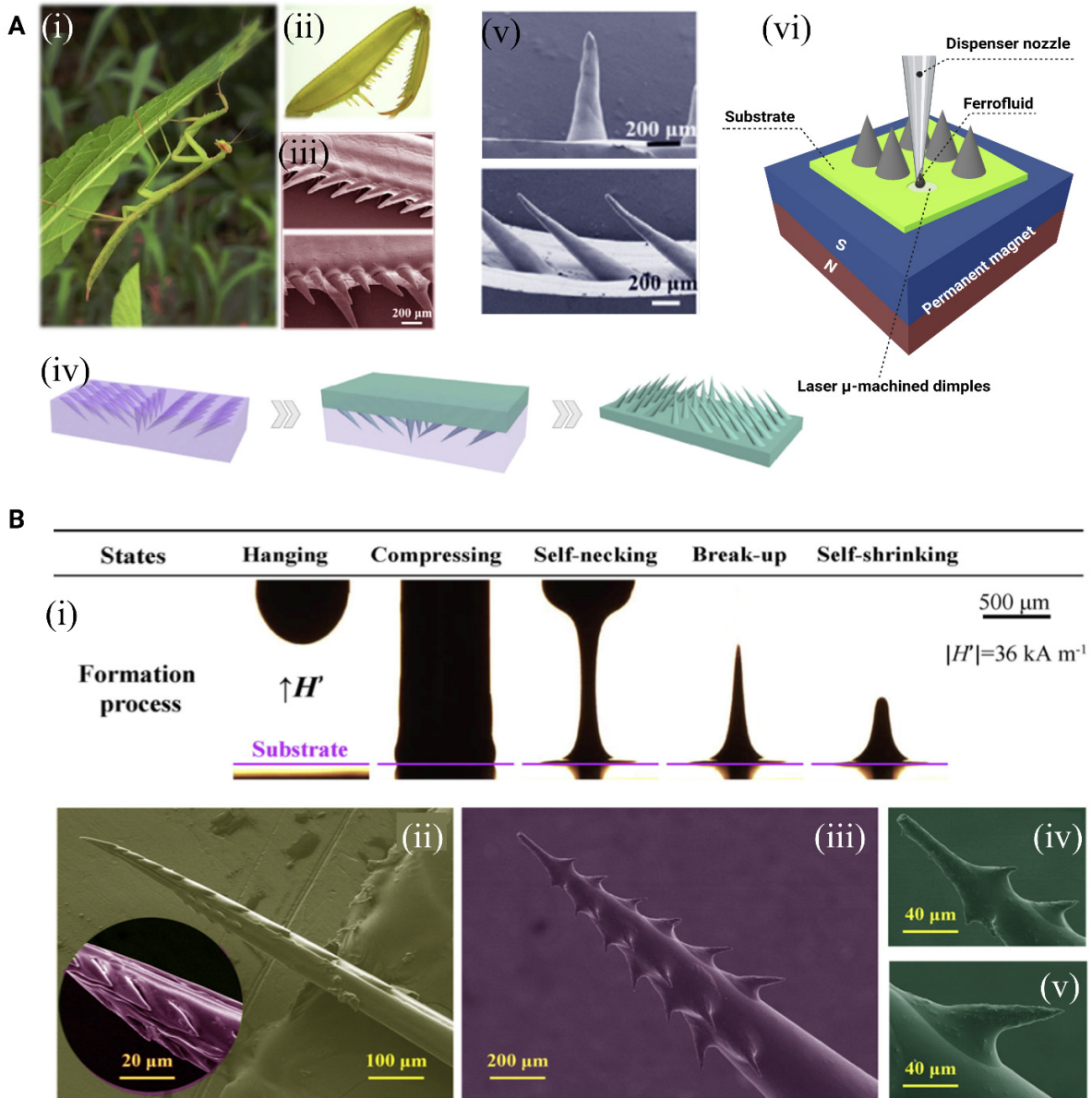


Figure 3 Fabrication approach using novel molding techniques. (A) Digital image of a praying mantis (i). Optical image of the serrated microstructures present on the forelegs of a praying mantis (ii). Scanning electron microscopy (SEM) images of the serrated microstructures (iii). (iv) Schematic of the microneedle manufacturing process using ferrofluid configured molds. (v) SEM images of the microneedle angles achievable using ferrofluids, ranging from 30° to 90° . Reprinted from ⁵¹ with permission from Elsevier. (B) Illustration of the fabrication process of a

liquid microneedle using the magnetorheological drawing lithography method (i). H' represents the external magnetic field. SEM images of a honeybee stinger-inspired microneedle manufactured using magnetorheological drawing lithography (ii-v). Reprinted from⁵⁴ with permission from Elsevier.

3.2.2 Magnetorheological drawing lithography

Magnetorheological drawing lithography (MRDL) offers solutions to some issues associated with the ferrofluid configured molding method. Whereas ferrofluid configured molding is a relatively complex manufacturing process, while MRDL is a simple and low-cost technique.⁵⁴ In addition, MRDL can produce extremely complex microstructures, one of the main limitations with ferrofluid configured molding. This technique uses a magnetic field to directly draw the 3D structure of a microneedle from a curable magnetorheological fluid. Specifically, microneedle preparation using magnetorheological drawing lithography is based on two key phases: an electrocapillary self-thinning phase and a magneto-capillary self-shrinking phase. A curable magnetorheological fluid droplet is initially suspended on a metal pillar and compressed on the substrate surface (**Figure 3B**). In the presence of an external magnetic field, the droplet is drawn back and subsequently deposited as a needle-like structure. This magnetic field is then maintained during the solidification process in which the needle is baked using an oven and hot air blowing. This technique may be adapted for fabricating microneedles on a 2D surface as well as BMNs in the 3D space. For example, BMNs based on a honeybee stinger have been manufactured using magnetorheological drawing lithography (**Figure 3B**). The curable magnetorheological fluid, composed of a modified aliphatic amine, epoxy novolac resin and iron power, was polymerized through condensation reaction at 80°C for 3 min.⁵⁴ This particular polymer yielded a solid microneedle that required a low penetration force and generated strong adhesive force.

3.3 Three-dimensional printing

Three-dimensional printing refers to a wide variety of additive manufacturing strategies that add materials step-by-step in an adjusted manner to fabricate a 3D object. These strategies are roughly classified into two types: extrusion-based 3D printing with a forming tool that controls material deposition and light-based 3D printing in which light illumination is used to create a 3D object. Fused deposition modeling, nozzle-based 3D printing and multi-jet modeling are examples of extrusion-based 3D printing. Stereolithography, selective laser sintering/melting, digital light projection, micro-stereolithography and two-photon polymerization are examples of light-based 3D printing.⁵⁵ **Figure 4A** lists the resolutions of well-known 3D printing techniques. The

advantages and limitations of conventional molding techniques and the different 3D printing methods are summarized in **Table 1**. It should be noted that 3D printing, especially two-photon polymerization, is a novel approach for the printing of microneedle patches. The 3D printers employed for printing are the same for the fabrication of both conventional microneedles and BMNs; only the design is different for the BMNs. The 3D printing technologies available for microneedle fabrication are used for BMN fabrication. Although advances in printing speed and resolution of 3D printers are incorporated into the design of BMNs, such a technology is still in its infancy state of development and there is ample room for progress. In this section, different 3D printing approaches are presented and compared in terms of resolution and speed, with highlights of the advantages and limitations of each approach.

Table 1. The advantages and limitations of conventional molding techniques and some 3D printing techniques that have been used for the fabrication of bioinspired microneedles.

Method	Fabrication process	Advantages	Limitations
Traditional molding methods	Solvent casting	<ul style="list-style-type: none"> • High reproducibility • High precision • Inexpensive • Easily scalable • High throughput • Compatable with many polymers 	<ul style="list-style-type: none"> • Difficult to produce complex structures • Multi-step manufacturing process • Requires low viscosity polymer solutions to achieve complete coverage of microholes during the vaccum process
	Casting and Polymerization	<ul style="list-style-type: none"> • High reproducibility • High precision • Scalable 	<ul style="list-style-type: none"> • Use of a chemical initiator • Limited materials • Geometry restrictions
Novel molding methods	Ferrofluid configured molding	<ul style="list-style-type: none"> • High reproducibility • Can generate MNs with inclination angles ranging from 30° to 90° 	<ul style="list-style-type: none"> • Complex manufacturing • Expensive • Difficult to produce complex MN designs
	Magnetorheological drawing lithography	<ul style="list-style-type: none"> • Inexpensive • User friendly process that can produce complex MN designs 	<ul style="list-style-type: none"> • Limited to solid or coated MN designs • Limited materials
3D printing methods	Fused deposition modeling	<ul style="list-style-type: none"> • Economical • User friendly • Multi-material printing 	<ul style="list-style-type: none"> • Slow printing • Low resolution and accuracy • Risk of drug degradation • Liquid permeation because of imperfect layer adhesion
	Stereolithography	<ul style="list-style-type: none"> • Smooth surface 	<ul style="list-style-type: none"> • Potential toxicity

	<ul style="list-style-type: none"> • High resolution • Applicable for hollow microneedle 	<ul style="list-style-type: none"> • Mechanical properties deteriorate over time • Supports are required in most cases
Digital light projection	<ul style="list-style-type: none"> • High resolution • Small structure with smooth surface • Printing each layer with one radiation 	<ul style="list-style-type: none"> • Potential toxicity • Supports are required in most of cases • Pixel size restriction • Mechanical properties deterioration over time
Continuous liquid interface production	<ul style="list-style-type: none"> • Rapid • High resolution • Uninterrupted printing 	<ul style="list-style-type: none"> • Expensive • Potential toxicity • Heat wastage in dead zone • Suitable just for oxygen-sensitive resins
Two-photon polymerization	<ul style="list-style-type: none"> • Ultra-high resolution • Direct writing with laser beam • Multiscale micro/nano structure • Biocompatible materials available • Fully 3D 	<ul style="list-style-type: none"> • Expensive • Mostly for small-sized printing sub-mm dimensions • Low scalability of the process

3.3.1 Fused deposition modeling

The fused deposition modeling technique prints a 3D object layer-by-layer by extruding a semi-molten thermoplastic material above its glass transition temperature. Although this method is inexpensive, widespread and user-friendly, the low resolution of the printed object confines its application in microneedle fabrication.^{56,57} Nevertheless, efforts have been made to overcome this limitation. Several parameters, including the printer nozzle diameter, printing temperature, layer thickness, part orientation, raster angle, air gap, extrusion width and infill extrusion width, have been adjusted to improve the quality of the printed object. The recommended adjustments for print microneedles are 0.2 mm layer thickness, 0.3 mm extrusion width, 0.2 mm infill width, 0.2 mm nozzle orifice diameter and 165°-185 °C nozzle temperature.⁵⁸ Proper post-printing techniques may also improve the final resolution of the printed microneedles. For example, chemical etching with an aqueous potassium hydroxide solution is a post-printing method which improves the resolution of the printed microneedles from tip sizes higher than 170 µm to tip sizes smaller than 55 µm. There are no adverse effects reported on the mechanical and material properties of microneedles.⁵⁹

3.3.2 Stereolithography

Stereolithography is a light-based layer-by-layer 3D printing method that has attracted the attention of researchers in microscale fabrication, including microneedles.⁶⁰ Stereolithography 3D printing utilizes ultraviolet light to illuminate a photosensitive resin tank to cure each layer. Resins such as castable resin,⁶¹ dental SG resin,⁶² clear resin⁶³ and class I resin^{64,65} have been employed for microneedle fabrication. After printing each layer, the mechanical elevator moves the platform vertically upward with a height that is equivalent to the thickness of each printed layer. The printer repeats this procedure to complete the 3D object (**Figure 4B-(i)**).⁶⁶ After printing, the item needs to be peeled off from the printer's platform and washed thoroughly with isopropanol alcohol to clean the remnant unsolidified resin. The printed object is further exposed to ultraviolet light for a specific time and temperature to ensure complete polymerization.⁶⁷

Stereolithography printing resolution is defined into two classes: a) vertical resolution, which corresponded to the layer thickness, and b) planar resolution, which corresponded to the 2D cross-section sketch. Although these resolutions depend on the printer's brand, printing resin, and printing time, the reported resolutions are almost identical (25 μm vertical and 140 μm planar).⁶⁸ To the best of our knowledge, the lowest reported radius of the printed microneedle tip is 18 μm .⁶⁷

Stereolithography is a precise microscale technology that has demonstrated acceptable results in printing hollow microneedles.^{65,69} However, microneedles that are printed by stereolithography are shorter than their counterpart designs with the same base diameters, with 10% difference in the tip radius.⁶¹ Moreover, increasing the length or aspect ratio (i.e. length-to-base diameter ratio) increases the discrepancy between the printed microneedles and their original design.⁶³

Bioinspired microneedles may be fabricated with stereolithography directly.^{61,65} Alternatively, this technology may be used to fabricate microneedle array basins to develop microneedle masters and finally fabricate the microneedle female mold via the "Print-and-Fill" strategy.⁶³ It is worth mentioning that stereolithography may be used to print multi-material items.⁷⁰ The technique can also be combined with other technologies such as inkjet printing^{64,68} or microelectromechanical systems⁶⁵ to enhance the drug delivery features of BMNs.

Micro-stereolithography is very similar to stereolithography in manufacturing principles, with improvement in resolution. Different factors affect the resolution of stereolithography. Vertical

resolution is related to light penetration of the polymerizable resin. The light beam should be confined to the surface and prevented from penetrating too deeply by a) reducing the exposure time to slightly longer than the required time for initiating the polymerization, and b) using photosensitive resins with high absorption of the irradiation wavelength. Although adapting the reactivity and optical thickness of a photochemical medium improves vertical resolution, it does not affect planar resolution, because the latter is not directly related to chemistry. Instead, planar resolution is related more to the light beam diameter and the accuracy of the scanning system. There are three potential solutions for increasing planar resolution: reducing the light beam spot size by increasing its focus, layer projection instead of scanning the light beam and solidifying directly inside the medium instead of on its surface.⁷¹ These improvements may also be used in other light-based 3D printing methods such as digital light projection, continuous liquid interface production and two-photon photopolymerization.

3.3.3 Digital light projection

High-precision digital light projection has been used to print microneedles. This method is precise enough to build microneedles and reduce their fabrication cost substantially.⁷² Microneedles fabricated with this method are used for sensing, sampling and injection.^{73,74} In this method, light with a specific wavelength, usually ultraviolet light, is used to light-cure a polymerizable resin. The 3D-designed model must be sliced to several 2D cross-section sketches with a given thin thickness to be exported to the projector. The projector focuses the polymerizing light on the digital micromirror devices (DMDs) through its lens. A DMD rectangular chip array comprises several hundred thousand microscopic mirrors.⁷⁵ The DMD reflects light to the resin and cures the freshly emitted layer. After printing each layer, the substrate moves vertically to a depth that is equal to the layer's thickness until the 3D model is completed. In this way, the first layer sticks to the substrate while all the other layers stick to their previous layer. The printed object requires post-processing to eliminate extra supports and rinsing off the developer.⁷⁶ **Figure 4B-(ii)** represents an abridged schematic of this technology.

Similar to stereolithography, the resolution of digital light projection is divided into two classes: vertical resolution and 2D resolution. The vertical resolution or layer thickness is between 20 and 100 μm . The 2D resolution is $50 \times 50 \mu\text{m}^2$.⁷⁷⁻⁷⁹ Although 2D resolution is limited by the

pixel size of the digital micromirror device, magnification optics can increase the resolution. Alternatively, larger objects with a lower resolution may be printed.⁸⁰

Exposure time plays an important role in the precision and stiffness of the printed object. Increasing the exposure time enhances the stiffness of BMNs and results in outputs larger than the original design. Conversely, a short exposure time does not provide enough light density to form solid microneedles and decreases the stiffness of the BMNs. Although increasing the exposure time may improve the construction of the needle base, it may be inadequate for microneedle tips. Experiments confirmed that a range of exposure times can result in acceptable printing of BMNs, which is 300-500 ms for a 0.7 mm long microneedle.⁷⁵ Any time longer than the acceptable range will result in extra solidification.

Both stereolithography and digital light projection utilize photopolymerization as the solidification strategy. However, they have substantial differences in the printing mechanism. Stereolithography utilizes an ultraviolet light-based laser beam and prints by polymerizing the resin dot-by-dot. In contrast, digital light projection employs an ultraviolet light projection source and prints by curing one layer at a time. Consequently, the printing speed of digital light projection is considerably faster. Unlike stereolithography, light source intensity is adjustable in digital light projection, which enables the user to control the light's effect.^{78,81,82}

Digital light projection is an additive manufacturing technology with layer-by-layer printing capability. However, it has been modified for the development of volumetric additive manufacturing (i.e. printing the entire object at once), which is a much more rapid approach ($>10^5$ mm³/h).⁸³ New volumetric printers are inspired by computed tomography, with the tomography technology utilized in reverse. Projections from many angles (0° to 360°) are calculated using a tomography algorithm. These projections are fed to the transparent resin by the digital light projection system as the resin container rotates. The cumulative polymerized volume of the resin reproduces the 3D object same as shown in **Figure 4B-(iv)**. The smallest printed size associated with this method used to be around 300 μm⁸⁴. However, a recent work improved the resolution to 80 μm by modifying the etendue of the illumination system and the resin viscosity.⁸⁵ Thus, volumetric additive manufacturing is a potential method for the production BMNs.

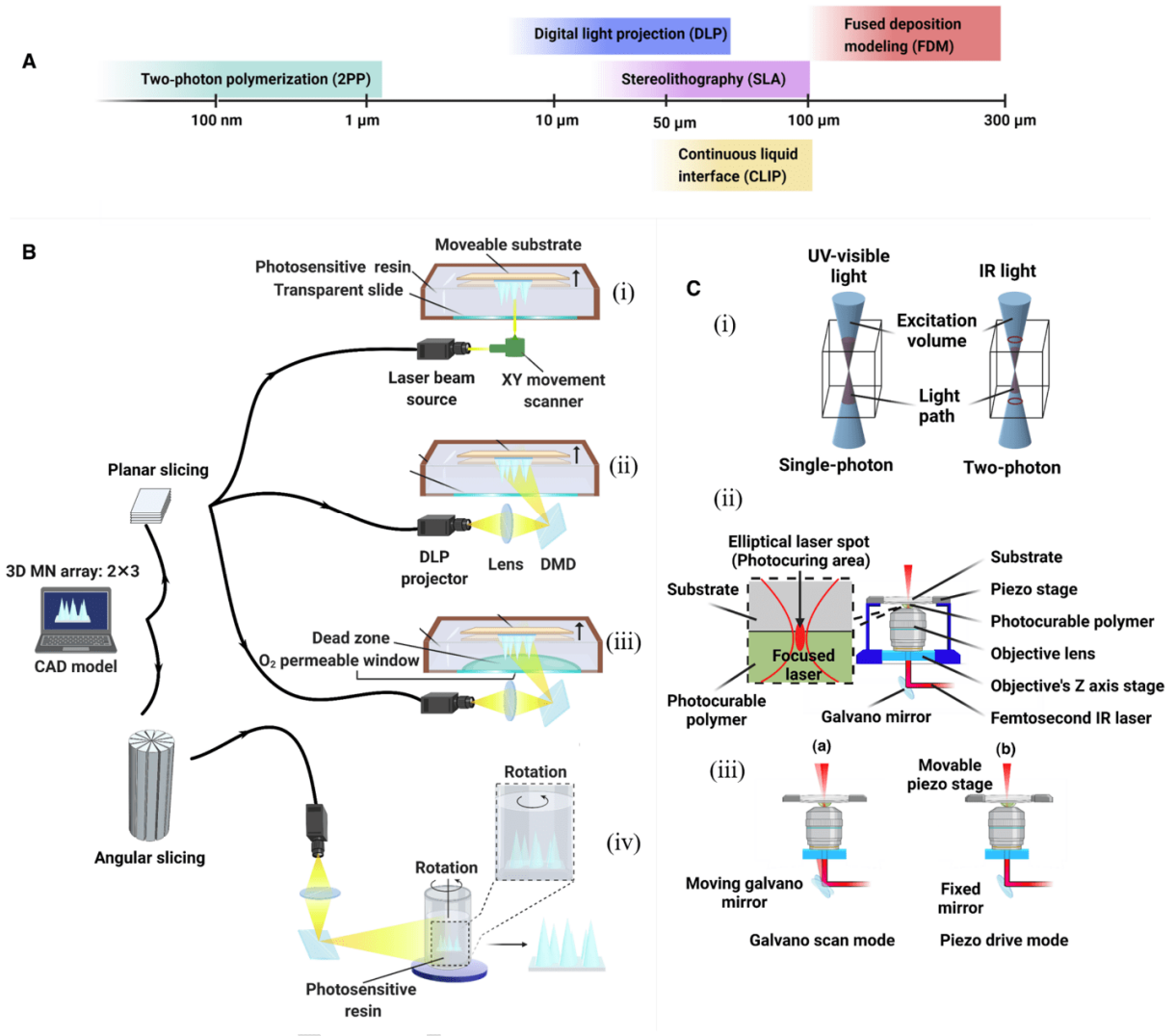


Figure 4 Light-based 3D printing techniques used for microneedle fabrication. (A) Resolution of different 3D printing methods. Two-photon polymerization has the highest resolution. Fused deposition modeling has the lowest resolution. The resolutions of stereolithography, digital light projection and continuous liquid interface production are similar.^{86–88} (B) Ultraviolet (UV) light is used in single-photon 3D printing. According to the layer-by-layer additive manufacturing strategy, the 3D model is sliced planarily or angularly. (i) A laser beam source provides polymerizing light via an XY movement scanner to solidify the resin dot-by-dot in stereolithography (SLA) printing. The vertical movement of the substrate makes it possible to print each layer over the previous layer. (ii) Although digital light projection (DLP) 3D printing is similar to SLA, each layer is created at one illumination employing digital micromirror devices (DMDs). (iii) The continuous liquid interface production (CLIP) technique is developed based on DLP. It is equipped with an O₂ permeable window which accelerates the printing procedure. (iv) Volumetric 3D printing method based on DLP and a rotating resin vat. (C) Two-photon polymerization is the most precise light-based technique. (i) Comparison between single-photon excitation volume and two-photon excitation volume. (ii) Overview of the two-photon polymerization device; focused laser beam polymerizes the photocurable resin through the Galvano mirror and objective lens. The structure is fabricated, sticking to

the piezo stage. (iii) Two different strategies are implemented for the 3D movement of the laser beam focus: (a) by moving the Galvano mirror and (b) by moving the piezo stage.

3.3.4 Continuous liquid interface production

This is a novel 3D printing method that is developed based on digital light projection. In this approach, light irradiates to the resin bath through an oxygen-permeable ultraviolet light-transparent window. As oxygen diffuses into the resin through the window, it inhibits polymerization and creates a thin “dead zone” layer where resin polymerization does not occur. Once the ultraviolet light is removed from the window, the oxygen density decreases and resin polymerization occurs. The dead zone eliminates mechanical delamination and additional coating steps. Consequently, the printing speed increases and the force applied on the printing subject is minimized.^{89–91} **Figure 4B-(iii)** illustrates the general concept of this 3D printing technology. Continuous liquid interface production is a rapid and tunable technique with high throughput, potentially pushing BMN production technology forward to the clinical setting phase.⁹² This method is 25-100 times faster than the original digital light projection although theoretically, it has the potential to print 1000 times faster than digital light projection.⁹³ Using continuous liquid interface production, a BMN patch may be printed in less than 10 min. This advantage makes continuous liquid interface production a much sought after 3D printing method for rapid production of an enormous library of microneedles with various sizes, shapes, aspect ratios, spacings and compositions for systematic investigations on the effects of microneedle geometry on clinical outcome.⁹² Because continuous liquid interface production prints BMNs shorter than their original design, rescaling the design with a factor larger than one in the Z-direction is required prior to BMN fabrication.⁹⁴ This technique can print microneedles ranging from 400 to 1000 µm in height, with tip radii close to 2 µm.⁹² Continuous liquid interface production may also be used to fabricate microneedle coating mask devices.⁹⁴

3.3.5 Two-photon polymerization

Two-photon polymerization is a 3D lithography additive manufacturing technology. This process has been largely implemented for the production of conventional microneedles^{95–107} and BMNs.^{13,108,109} This method is flexible, highly precise and time-effective.¹⁰⁴ Two-photon polymerization is capable of printing objects on the centimeter-scale with submicron resolution (~100 nm).⁸⁶ Different materials may be used to fabricate BMNs via two-photon polymerization.

Examples of these materials include modified ceramics^{95,98}, inorganic-organic hybrid polymers^{99,109}, acrylate-based polymers^{100–102}, polyethylene glycol¹⁰³ and water-soluble materials.⁹⁶ The previously described 3D lithography methods that print with ultraviolet light radiation are classified as single-photon strategies. In contrast, two-photon polymerization uses short-pulsed laser radiation in the range of visible to near-infrared light, combined with the nonlinear effects of two-photon absorption. In single-photon polymerization, the reaction occurs in all the light-exposed areas. Conversely, multi-photon polymerization occurs only in the area in which multi-photons are continuously absorbed (**Figure 4C-(i)**). Accordingly, the resolution of multi-photon lithography is much more precise. Two-photon polymerization fabricates 3D structures by direct laser writing inside a transparent photocurable polymer (**Figure 4C-(ii)**). Two-photon absorption induces a limited photochemical reaction to polymerize the photocurable polymer within the focus volume of a highly-focused laser beam. Control of 3D movement via laser beam focusing makes it possible to print 3D objects with resolution lower than 100 nm.¹¹⁰ **Figure 4C-(iii)** illustrates the two different modes utilized in the Nanoscribe GT system (Nanoscribe, Karlsruhe, Germany) to move the laser beam focus, with the galvano scanning mode being 100 times faster than the other.¹⁰⁴ It is worth mentioning that the printing resolution does not depend on the resolution of the piezo stage movement or the galvano scanning resolution. Rather, it depends on the curable range of the photocurable polymer in one-time radiation of the laser beam.¹³ Two-photon polymerization is not restricted to layer-by-layer printing. Thus, it offers more flexibility and the ability to print a wide range of designs. Print quality is affected by slicer parameters, laser input, post-development treatment, material choice, writing field size, scaffold size and block size.^{98,104}

Two-photon polymerization is capable of printing BMNs with different fabrication strategies and geometries. Hollow microneedles equipped with drug reservoir, with an aspect ratio (height/outer diameter of the microneedle tip) ranging from 1 to 20, were printed directly with two-photon polymerization. The inner diameter and height of the microneedles ranged from 80 to 120 μm and from 200 to 400 μm , respectively. The wall thickness at the tip of the microneedles was 5 μm .¹⁰⁶ Another example is ultra-sharp tip hollow surgical microneedles printed directly by two-photon polymerization.¹⁰⁷ This method can print multi-part BMNs inspired by nature.¹³ Two-photon polymerization is also a powerful method for printing master templates to be used for

manufacturing microneedles via the casting method.^{96,102,104,105} One example is the master template of hollow microneedles with an open channel along the side of the body. These hollow microneedles measure 700 µm from the tip to the of the needle and have an internal diameter of 30 µm.⁹⁷

3.4 Four-dimensional printing

Conventional fabrication methods such as molding are difficult and costly for creating complex structures. Recent 3D printing techniques have made it possible to fabricate nanoscale microneedles with high resolution and complex geometries. However, their typical stepwise, layer-by-layer printing creates limitations in the fabrication of complicated structures. Although inserting supports and rotating the design may improve printing capability, the problem is still incompletely resolved especially when attempts are contemplated to imitate mother nature.¹¹¹ Furthermore, employing supports in microscale 3D printing is not feasible in 3D printing that involves multiple materials and sacrificial printable materials.¹²

Four-dimensional printing is one step beyond 3D printing. This method utilizes stimulus-responsive materials for printing.¹¹² These smart materials respond to different types of stimuli including physical, chemical and biological stimuli (**Figure 5A**). Some of the materials employed in 4D printing are responsive to multiple stimuli such as thermo-magnetic, thermo-pH, thermo-light or thermo-humidity stimuli (**Figure 5B**).¹¹³ The post-printing shape-changing response to those stimuli may be in the form of bending, elongating, twisting, corrugating or a combination of these deformations.¹¹⁴ In this way, a 3D printer fabricates a simpler prototype of the final design through the use of an appropriate smart material. Additional complexities can be created in the printed object via the application of controlled stimuli.

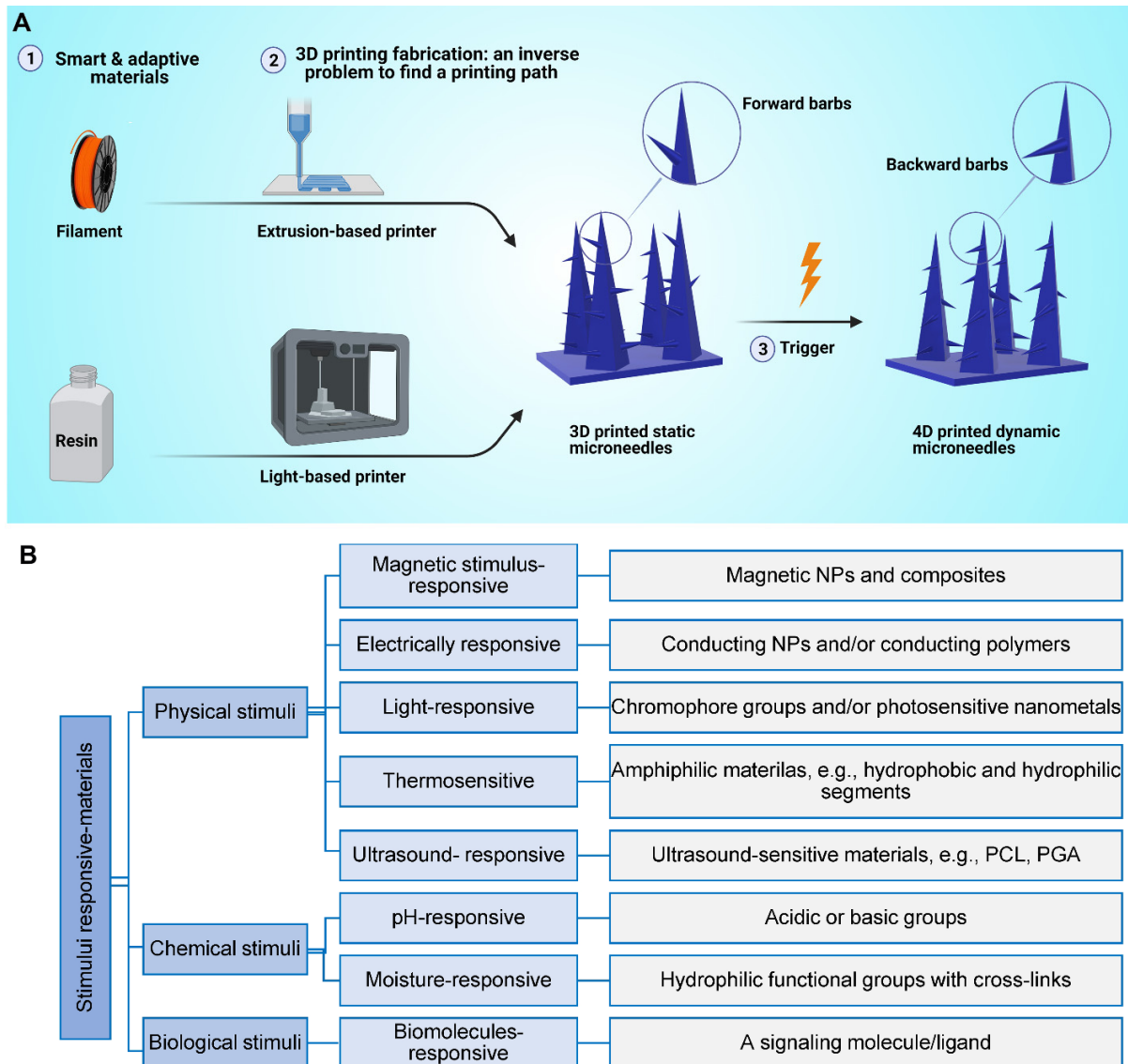


Figure 5. Four-dimensional printing of a BMN array. As a new fabrication method, 4D printing utilizes smart materials to develop 3D-printed structures with controllable post-printing deformations. A) General concept of 4D printing. B) Classification of smart materials and their associated stimulus. NP: nanoparticles; PCL: polycaprolactone; PGA: polyglycolic acid. Part B modified from ¹¹³ from ACS Publications under open access license.

The idea of microneedles equipped with backward-facing barbs was inspired by the honeybee stinger. This is an example of a complex structure with a challenging fabrication protocol. The fabrication of such a complex microneedle is almost impossible using existing 3D printing methods, except for the use of magnetorheological drawing lithography. However, the latter is a complicated, expensive and time-consuming 3D printing method.¹¹⁵ The use of a 4D printing approach may overcome these difficulties. Microneedle arrays with undeformed barbs are printed with digital light projection followed by irradiation of ultraviolet light on the microneedles (**Figure 6**). Irradiation initiates photopolymerization at the microneedle surface which propagates inside the resin. Because the precursor resin reduces irradiation density, the cross-linking density of the polymerized resin decreases from the surface to the interior. During printing, the barbs remain horizontal. Post-printing rinsing with ethanol removes uncured monomers from the bottom section of the barb. The uncured resin monomers diffuse out, leaving behind loose spaces. This results in shrinkage at the bottom of the array during drying and causes the barbs to bend downward. Subsequent exposure to ultraviolet light stabilizes the deformed shape of the barbs.¹²

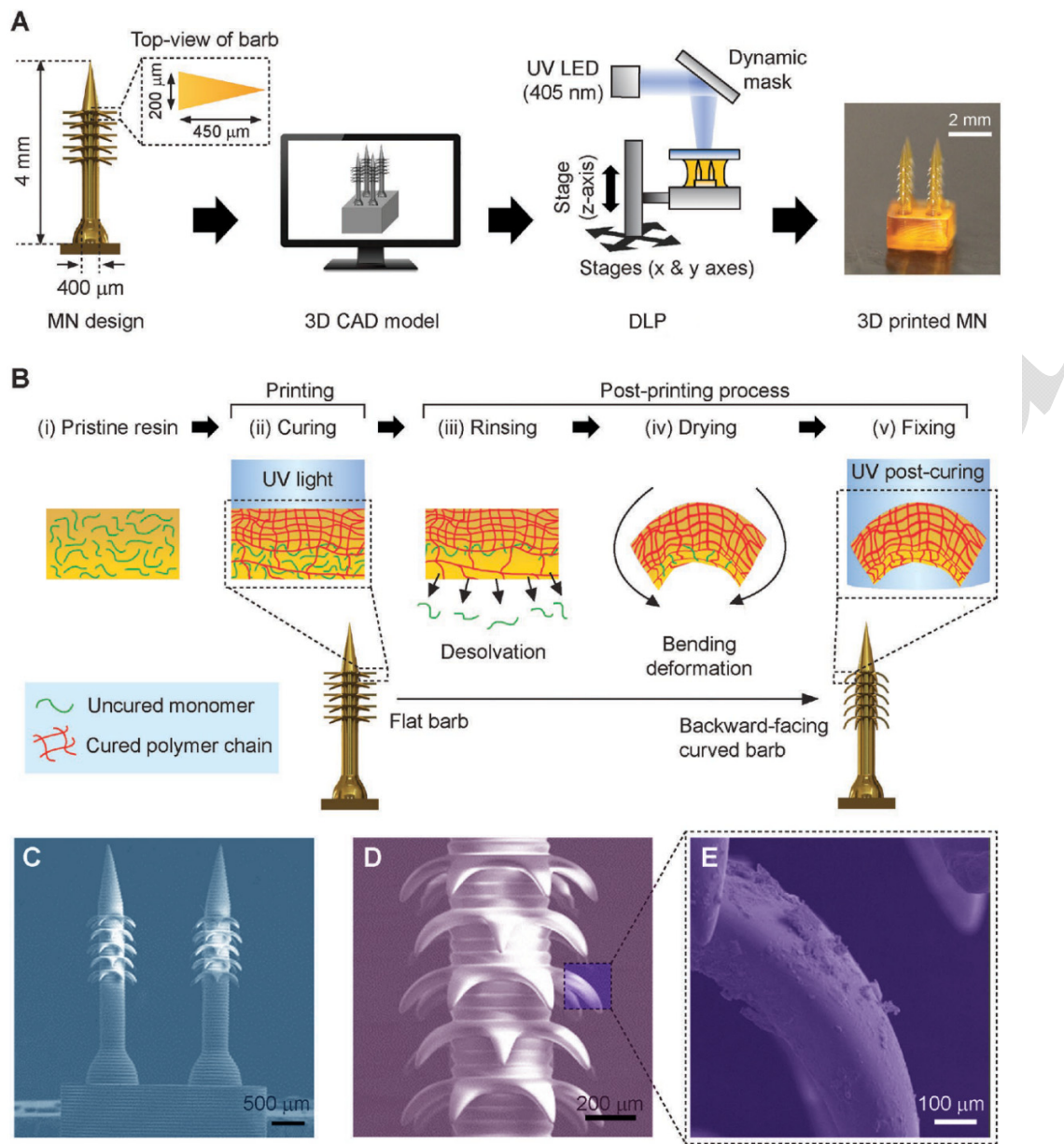


Figure 6 (i) Digital light protection printing of BMNs with horizontal barbs. (ii). Use of the 4D printing approach to create backward-facing deformation in barbs. (iii) SEM images of 4D-printed BMNs with backward-facing barbs. Reprinted from ¹² with permission from Wiley.

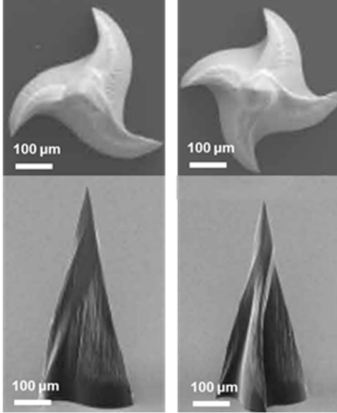
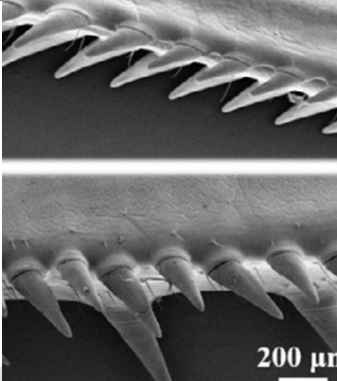
4. Bioinspired microneedles: Toward boosting performance and application

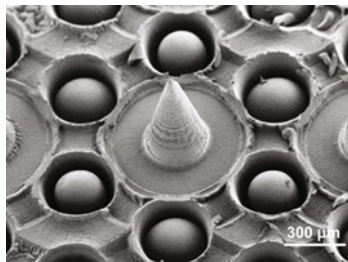
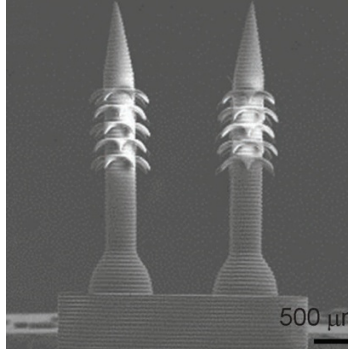
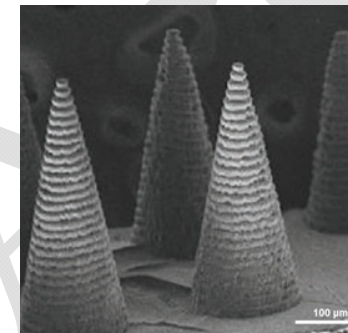
This section covers the diverse biomedical applications of BMNs. For each study, the inspiration for creating the destined BMN is given in detail. In addition, the efficacy of each BMN in fulfilling its biomedical application, such as wound repair, transdermal drug delivery, or both,

is described. In some studies, the BMNs may be used simultaneously for multiple purposes such as tissue adhesion and biosensing. **Table 2** summarizes the functionalities and architectures inspired by nature to create BMNs.

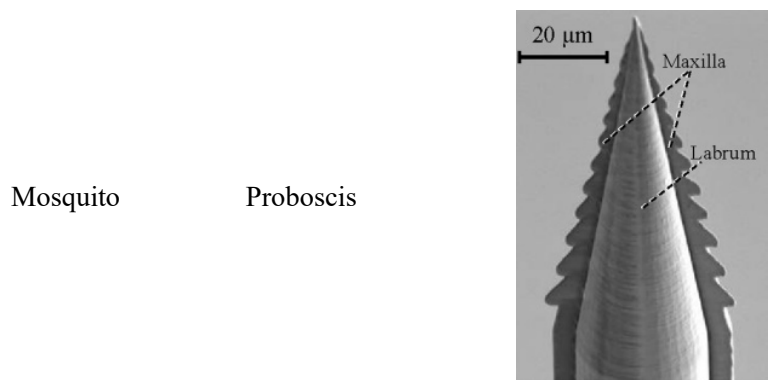
Accepted

Table 2 Representative BMNs for biomedical applications.

Inspirational source	Biomimetic organ/tissue	Image of bioinspired microneedles	Application	Major achievements and comparison with conventional microneedles	Ref
Snake	Fang		Transdermal drug delivery	<ul style="list-style-type: none"> -Grooved design of the snake fang-BMN patches allowed for rapid cargo delivery. -Single administration of influenza virus and ovalbumin antigen using the multi-grooved BMN patches induced robust protective immune responses in mice. 	⁷
Mantis	Forelegs		Tissue adhesion and transdermal drug delivery	<ul style="list-style-type: none"> - The mantis foreleg-inspired microstructures firmly adhered to the skin and remained attached in the presence of external forces. This helped to overcome limitations associated with conventional microneedles (i.e. easily falling off from the skin during motion). - Glucocorticoid-loaded serrated BMNs exhibited enhanced efficacy in treating imiquimod-induced psoriasis in mice. 	⁵¹

Mussels and octopi	Mussels – adhesive protein of mussel byssi Octopi – suction cups		Tissue adhesion and transdermal drug delivery	<ul style="list-style-type: none"> -The mussel- and octopus-inspired BMNs could bear 60 gm weight objects >240 times their own mass. -The BMNs adhered to porcine skin when it was lifted, bent, sprayed with or immersed in water. - Glucocorticoid-loaded suction cup BMNs assisted in healing cartilage lesions, reduced inflammatory cell infiltration and decreased fibrosis in a knee osteoarthritis model. 	49
Honeybee	Stinger		Tissue adhesion and transdermal drug delivery	<ul style="list-style-type: none"> -Pull-out force of the backward-facing barb-inspired BMNs was 18 times higher compared to barbless microneedles. - Maximum pull-out force increased when the number of barbs and the number of barb rows increased. 	12
Limpets	Tooth		Transdermal drug delivery	<ul style="list-style-type: none"> - The 2.5% aligned iron oxide (aIO)-based composite BMNs punctured artificial skin without buckling. In contrast, the pure polymer microneedles buckled during insertion. The BMNs were capable of overcoming the poor mechanical properties of conventional microneedles. - Mouse studies showed that there were no pain-associated behavioral changes after application of the BMN patches. 	11

European true bugs	External scent efferent systems		Transdermal Drug/vaccine delivery	- When a drug/vaccine was loaded at the base of the BMNs, the oriented microarrays directed the cargo toward the microneedle tip in a unidirectional manner. This design holds great promise for controlled drug delivery. ¹⁰⁹
Flower	Petal surface		Transdermal bio-sensing	- A surface-enhanced Raman spectroscopy (SERS) biosensor was developed in the form of nanoflower-like BMN for transdermal sensing. ¹¹⁶ - Au was successfully deposited on the HA-coated BMNs. These BMNs possessed high surface area to generate a SERS effect.
Endoparasites	Swollen proboscis		Tissue adhesion	- Through a shape change-mediated mechanically interlocking mechanism, BMNs showed universal adhesion to soft tissues and mechanically interlocked with tissues without inducing significant damage. - Easy encapsulation of a model drug was realized by the endoparasite-mimicked BMNs.



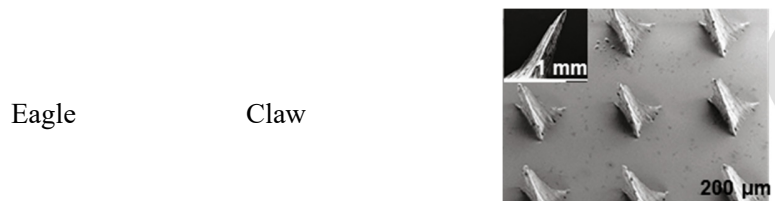
Skin insertion

- The BMN punctured artificial skin without buckling.

13

- Alternate vibratory motion of the two halves was imperative for reducing resistance force during needle insertion.

- The BMNs were capable of collecting human whole blood by capillary force for blood glucose measurement.



Tissue adhesion and wound healing

- The eagle-claw-inspired BMNs fixed and tightened the skin near a linear wound to prevent wound dehiscence.

- Liquid metal encapsulation into the BMN and its link to an external power source resulted in accelerated wound healing compared to the microneedle patches containing no liquid metal.⁸

4.1. Drug delivery

Technical limitations restrict conventional microneedles from delivering drugs in liquid form. This is because solidification of the liquid formulations reduces the activity of the loaded drugs/vaccines.¹¹⁷ Rear-fanged snakes have open grooves on the surface of its fangs. This ingenious venom delivery system enables them to quickly inject venom into the prey's tissue without creating excessive pressure on its Duvernoy's gland during venom delivery (**Figure 7A-i**). In contrast, front-fanged snakes that possess hollow-tube fangs have to use high pressure on the venom gland to inject their venom into a prey's tissue with high surface energy.^{118,119} Inspired by the mono-grooved fangs of rear-fanged snakes with rapid capillary force–driven delivery system, a BMN patch containing multiple open grooves on the surface of needles was designed and fabricated (**Figure 7A-ii, iii and iv**).⁷ Such a bio-inspired platform enabled transdermal delivery of a variety of drugs and vaccines in liquid form, using gentle thumb pressure without the need for a complex pumping system. Tri-, tetra-, penta- and hexa-open grooved snake fang mimicking–BMN patches were prepared using photolithography. As shown in **Figure 7A-ii-iv**, the BMNs that contained more grooves were taller than those with fewer grooves. In addition, all needles were capable of piercing mouse skin. The maximum depth of needle insertion was achieved by the hexa-grooved BMN patch. With increasing penetration depth, larger holes were created in the skin. Penta-grooved snake fang–inspired open groove architectures were selected for *in vivo* studies. This is because the hexa-grooved version had the shortest groove length and was perceived to adversely affect liquid delivery into the skin.⁷

Transdermal liquid drug delivery using the multi-grooved BMN stamping patches was investigated by fluorescein isothiocyanate (FITC)/bovine serum albumin (BSA)–loaded patches *in vivo*. The FITC-BSA was rapidly delivered into the skin of mice within 15 seconds after needle insertion. Prolonged cargo delivery was realized by the snake fang–BMN patches as well. Investigation on diffusion of the cargo into the skin showed that fluorescence intensity of FITC-BSA was similar before and after patch removal. After removal of the BMN patch, the intensity of FITC-BSA decreased gradually, which was indicative of sustained diffusion of the fluorescein-conjugated protein into the skin of the mouse **6A-ii and iii**. It was further demonstrated that a single administration of influenza virus and ovalbumin antigen using the snake fang–BMN patches induced robust protective immune responses in mice and guinea pigs.⁷

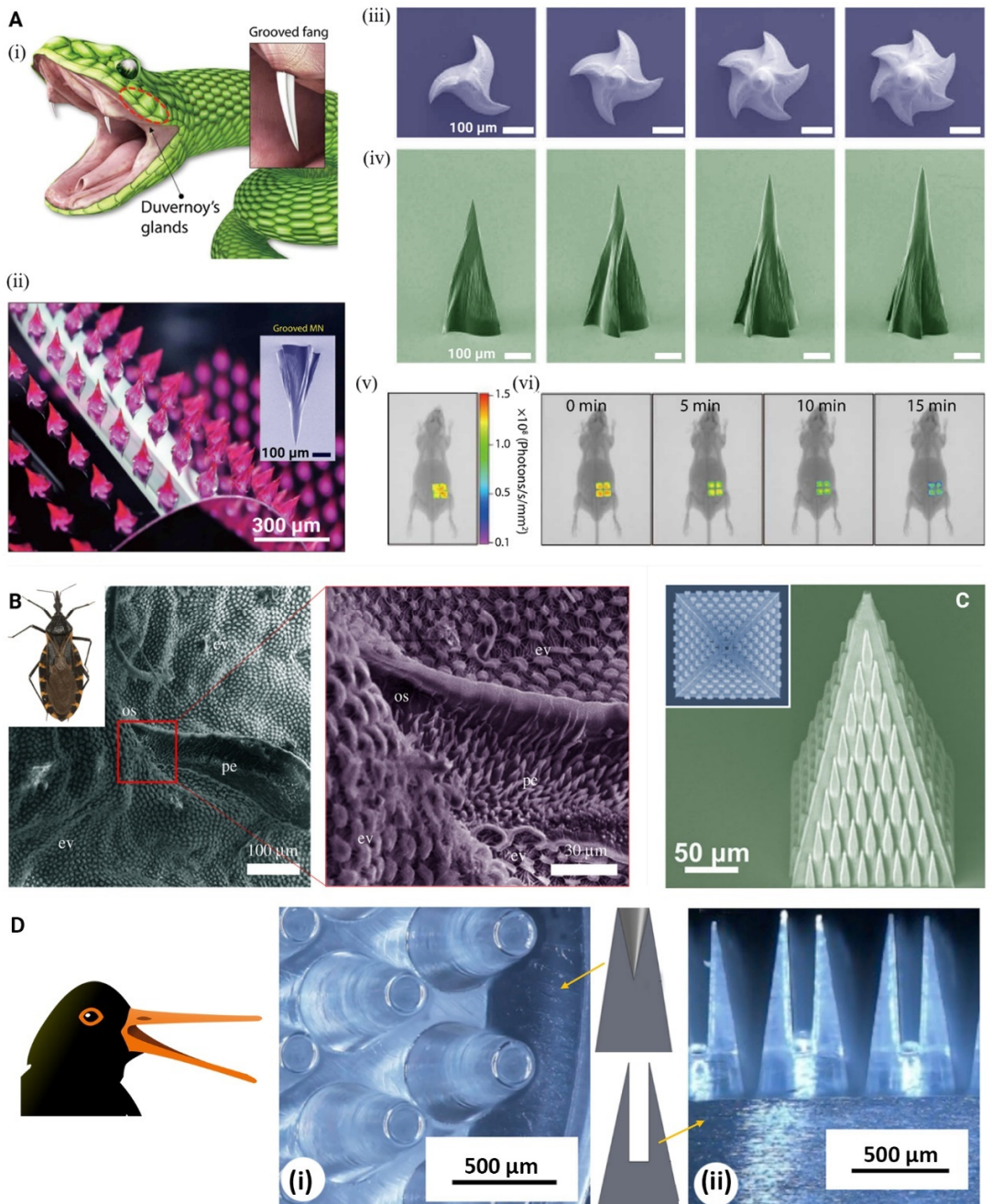


Figure 7. BMNs for drug delivery. **A)** (i) Illustration of the venom delivery system of a rear-fanged snake. (ii) Photograph of the snake fang-emulated BMN patch. SEM images of the top (iii) and side (iv) of the tri-grooved, tetra-grooved, penta-grooved, and hexa-grooved BMNs. In vivo fluorescence images before (v) and after (vi) removal of the fluorescein isothiocyanate-bovine serum albumin-loaded snake fang-BMN patch. Insertion time of the BMN was 15 s in the experiment. Reprinted from⁷ with permission from AAAS. **B)** *Rhaphigaster nebulosa* (common name: mottled shieldbug) and scanning electron microscopy of its body surface showing the ostiole (os), the peritreme (pe) and the evaporatorium (ev). Reprinted from¹²⁰ by the Royal Society under the terms of the Creative Commons Attribution License. (H) Optical microscopy images of an individual microstructure (left panel **C**) SEM image of the shieldbug-inspired microneedle (in

inset top view of the microneedle). Reprinted from¹⁰⁹ under open access license. **D)** Bird-beak bioinspired microneedle array. Design and photograph of (i) a semi-hollow microneedle and (ii) bird-beak mimicking BMNs. Reprinted from¹²¹ with permission from Springer.

Another BMN design mimicked the serrated microstructure of the praying mantis' forelegs. These serrated microstructures endow the praying mantis with excellent grasping and holding properties. This results in the creation of a novel serration-like clamping microneedle array that was fabricated by ferrofluid configured molding.⁵¹ The use of ferrofluids enabled negative micro-hole array molding with various sizes and angles toward the midline to be created easily and efficiently in a cost-effective manner. Such a design and fabrication method enabled the BMN to firmly adhere to the skin and remained attached even when subjected to external forces. The improved adhesion properties of the BMNs were demonstrated by the application of the microneedles at different inclination angles to the flanks of mice. The serrated clamping BMNs remained well attached to the skin when the mice were moving constantly. To evaluate the potential for drug release from the BMNs, fluorescein-coated BMNs and rhodamine B-coated BMNs were inserted into fresh porcine skin. After BMN removal, fluorescence was detected at the insertion sites of the BMNs. Three hours after BMN application, the depth of fluorescein penetration was three times deeper than the initial post-insertion depth. In another experiment, glucocorticoids were encapsulated within the serrated BMNs. The glucocorticoid-loaded BMN arrays significantly enhanced the delivery of glucocorticoids and their bioabsorption, thereby accelerating treatment of imiquimod-induced psoriasis in mice.⁵¹ This type of mantis foreleg-inspired microstructures is inspirational in overcoming the shortcomings associated with conventional microneedles that readily fall off the skin in the presence of external forces or during motion.

The endoparasite *Pomphorhynchus laevis* anchors to the intestinal wall of its host via a proboscis, immobilizing itself through swelling of the proboscis.⁴¹ Enthused by this feature, biphasic BMN patches have been developed that are capable of mechanically interlocking to tissue through their swellable microneedle tips.¹⁴ This unique design is used to produce self-adherent soft tissue BMN patches with minimal damage and reduced risks of infection, as well as sustained drug release.^{14,42} The adhesive performance of the BMNs was optimized by altering the swelling capacity of the needle's outer layer and the needle shape (e.g. cone vs bullet). The bullet-shaped swellable BMNs possessed improved adhesive property compared to the cone-shaped swellable BMNs. The BMNs with 60% swellable tip heights exhibited the greatest adhesion strength.⁴² In

an *in vivo* study on mice utilizing insulin-loaded BMNs, the blood glucose levels in the swellable BMN group gradually reduced. There were no clinical signs of inflammation or irritation at the insertion site.⁴²

Drugs or vaccines are usually loaded onto microneedle patches by spraying or dipping methods. The drug loading efficiency of these methods remains low. In nature, some insects possess droplet-shaped and open-capillary structures for movement toward the destined site (**Figure 7B**).^{109,122} Such structures allow them to spread a defensive fluid to protect them against predators.¹²³ Gland channels and microstructures can transport diverse liquids (aqueous and oil-based solutions) passively.¹²⁰ Hence, a microneedle patch was designed based on European true bugs (*Heteroptera*) (**Figure 7C**).¹⁰⁹ Inspired by these bugs, pyramid-shaped BMNs with their lateral faces covered by an array of tiny bug-inspired conical microstructures were constructed by two-photon polymerization lithography to mimic the secretory systems of the bugs.¹⁰⁹ *Ex vivo* human skin insertion was confirmed by methylene blue staining and optical coherence tomography. Nevertheless, only six of nine marks were present on the methylene blue-stained skin. This was attributed to the skin's irregularity and elasticity, which led to incomplete microneedle insertion. The BMNs could be removed intact from the skin. When a drug/vaccine was loaded at the base of the BMNs, the oriented microstructures directed the liquid-containing cargo toward the microneedle tip until the solvent evaporated. This left behind a portion of the cargo that was ready for use. This elaborate architecture facilitated the transport of a drug/vaccine to the needle tip in a unidirectional manner and provided the blueprint for the design and construction of advanced drug delivery systems that utilize BMN patches in a precise and controllable manner. Other nature-inspired designs have been fabricated for creating micropores in skin or enhancing the drug or gel coating. For example, semi-hollow microneedles created uncollapsed micro-holes on the stratum corneum for an extended period. Likewise, bird-beak bioinspired microneedles were capable of loading a coated gel (~ at the highest capacity of 3.2 ± 0.2 mg per MN array).¹²¹ **Figure 7D** shows the design and photographs of bird beak-inspired microneedles.

Tissue adhesion is also an important property for long-term drug delivery or detection. Although microneedle patches have been used as painless and noninvasive drug delivery systems, their poor adhesion and antimicrobial activity limit the clinical applications of conventional microneedles.¹²⁴ These limitations may be mitigated by the development of BMNs. In a recent study, BMNs inspired by mussels and octopuses have been synthesized (**Figure 8A**).⁴⁹ Mussels

adhere to surfaces based on covalent and noncovalent chemical interactions between an adhesive protein derived from the mussel byssi and the substrate.^{125–127} Octopuses use their suction cups and inner dome-like protuberances to adhere to both wet and dry surfaces.^{128,129} These natural, resourceful features have been harnessed in the BMN design (**Figure 8A-i, ii**). The BMNs were fabricated with a polydopamine hydrogel as the microneedle base and a loop of suction cup-resembling concave chambers that surround each microneedle. Polymyxin was loaded into the hydrogel tips and the polydopamine base to render the tips and base antimicrobial against common bacteria such as *Escherichia coli*. The BMNs were capable of bearing objects as heavy as 60 g, which was over 240 times of their own mass. The BMNs were able to adhere to porcine skin when lifted, bent or after immersion in water. They could also adhere to a thumb bent at 90° and remained in place when water was applied from above (**Figure 8A-iii**).⁴⁹ The suction cup-bearing BMNs that were loaded with glucocorticoid were further tested in a knee osteoarthritis model. Knee joints treated with the drug-loaded BMNs had less severe lesions, less inflammation and less swollen joints with greater flexibility compared with unloaded suction cup-bearing microneedles (**Figure 8A-iv**).⁴⁹ Examination of stained tissue slices confirmed that the drug-loaded suction cup-bearing microneedles promoted healing of cartilage lesions, reduced inflammatory cell infiltration, decreased fibrosis and reduced formation of cell clusters.

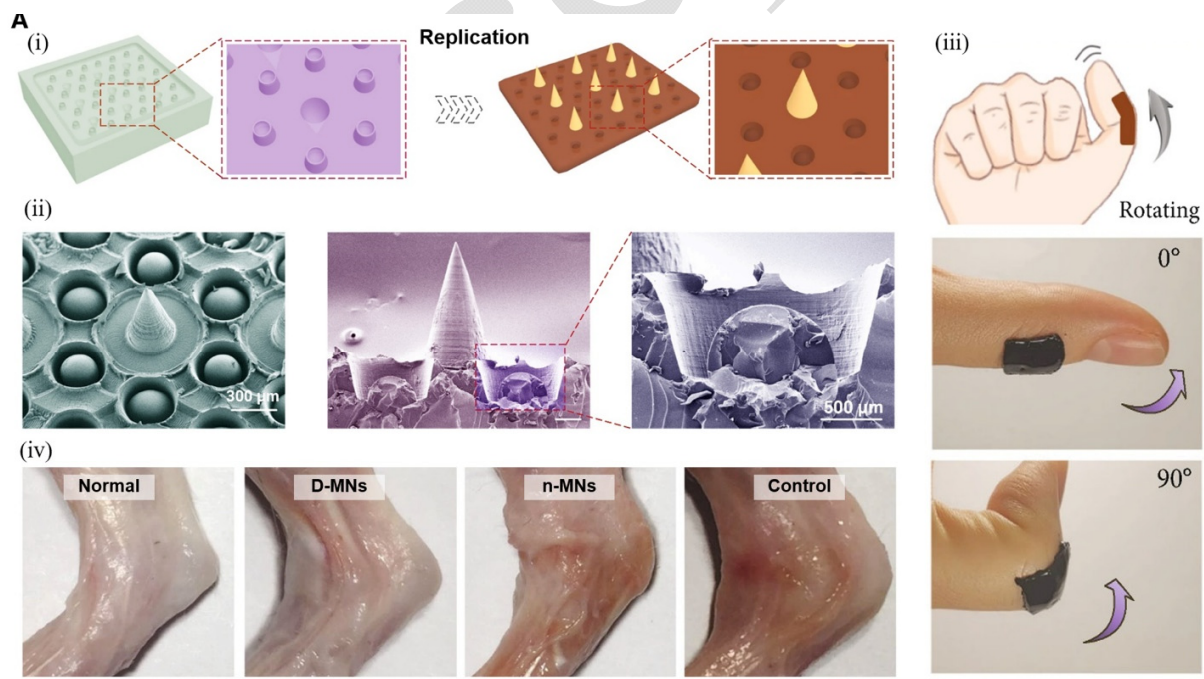


Figure 8. Octopus-inspired BMNs. Schematic of the microneedle fabrication process (i) and SEM images (ii) of the suction cup-resembling concave chambers. (iii) Diagram and photograph of the multi-functional BMNs adhering to the knuckle of the thumb when the knuckle was bent to 90°. The thickness of the BMNs was 2 mm. (C) Photographs of the knee joints of rats in different knee osteoarthritis treatment groups: normal group, glucocorticoid-microneedle group, unloaded-microneedle group and the control group, respectively. Reprinted from ⁴⁹ with permission from AAAS. d-MN: glucocorticoid-loaded MNs, n-MN: unloaded MNs.

4.2. Wound healing and regenerative medicine

Wound closure is an imperative aspect of wound healing. Improper wound closure around internal organs is particularly challenging because of the leakage of air and fluid. In addition, the reduced blood flow results in improper wound healing.^{130,131} Inspired by endoparasites that swell their proboscis to anchor to the host's intestines, researchers developed a hydrogel-based BMN patch that consisted of a non-swellable silk fibroin-based core and a swellable mussel adhesive protein-based shell for improved wound closure and healing (**Figure 7A-i**).⁴³ The biphasic structure of the BMN ensured that there was sufficient surface adhesion and needle stiffness for effective tissue insertion. The fracture force of the BMNs was 7-fold higher than the force required for porcine skin insertion. The needles are optimal for human skin insertion because porcine skin is 2.5- times more resistant to insertion than human skin.¹³²

A 3 cm-long full-thickness incision of the rat skin and a 5-mm diameter rat ileum defect model were used to determine external and internal wound closure, as well as the healing effects of the BMNs. In the external wound closure study, improved wound appearance was observed in the group treated with BMN patches after removal of the patches at 4 days post-surgery. In contrast, a thick scar and a readily identifiable rejoining mark were observed in the non-treated and suture-treated wounds, respectively (**Figure 9A-ii**). The superior performance of the BMNs was also confirmed by histological studies. As shown in **Figure 9A-iii**, the ultimate wound-breaking strength was ~3 times higher than that of suture-closed wounds at 21 days.

For healing of internal wounds, the tight sealing and liquid-absorption properties of the BMN patches enabled immediate arrest of hemorrhage with minimum tissue damage in the intestinal wounds. In contrast, there were obvious leakage and abscess formation in the abdominal tissues and adjacent intestines of the non-treated group at 14 days post-surgery. These unpleasant

phenomena were minimized in the BMN patch-treated group and there was 100% survival together with increase in body weight.⁴³

Researchers also employed FITC-dextran as a model drug to demonstrate the transdermal drug delivery potential of the biphasic hydrogel-based BMNs. The model drug was found to permeate into the deeper dermal regions over time by diffusion from the interstitial fluid-absorbing BMNs and proteolysis. The authors postulated that a BMN patch could be used simultaneously for enhancement of wound healing and for transdermal drug delivery.⁴³ The tissue adhesion capability of the BMNs may also be employed for tissue fixation and rapid hemostasis (**Figure 9B**).⁵⁰ In another study, a hierarchical design of feet or stings of insects that resembles a pagoda was used to produce a BMN patch to arrest hemorrhage. Such a design enabled the patch to attach strongly to various organs through mechanical interlocking.⁵⁰

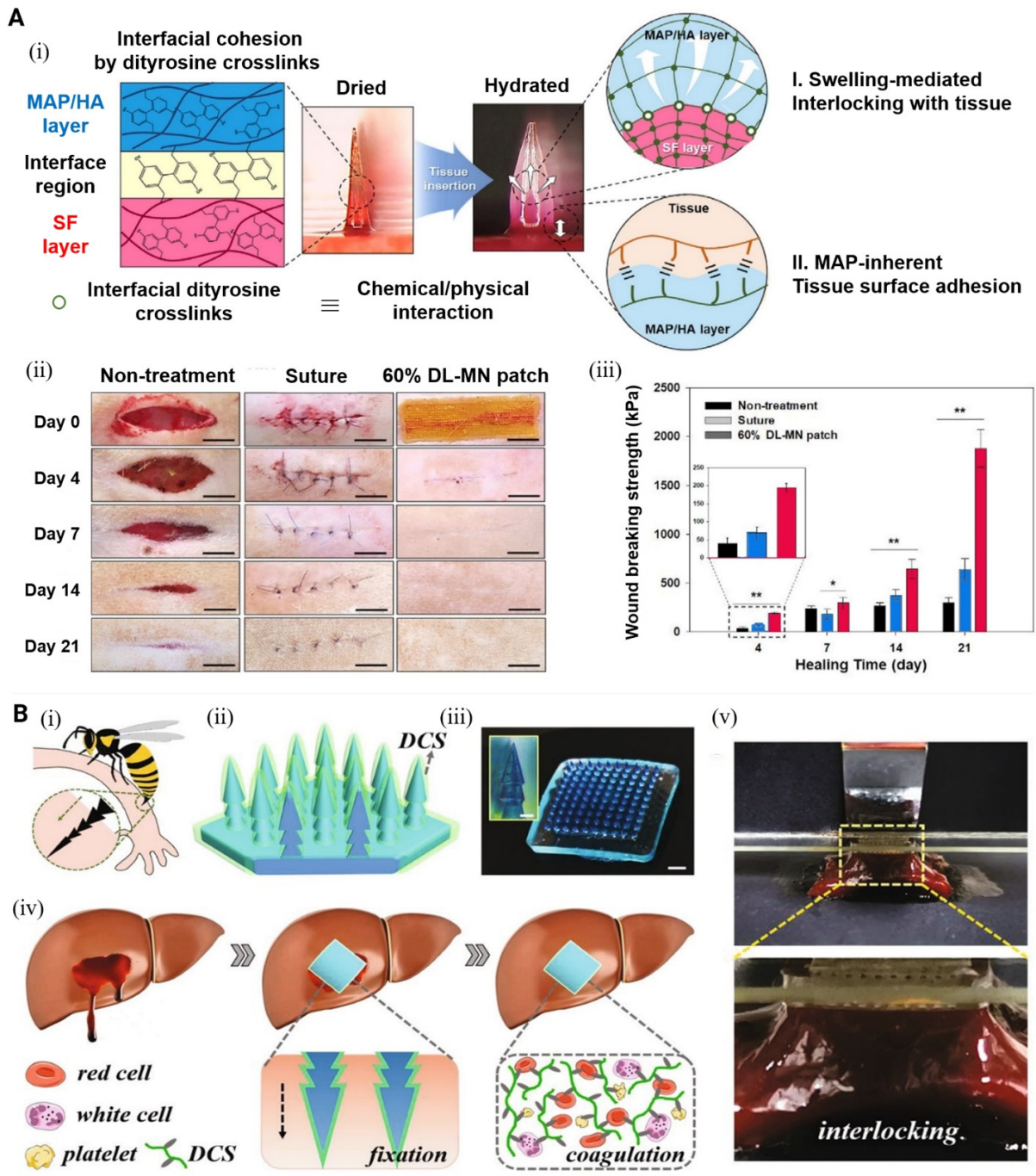


Figure 9. Bioinspired swellable hydrogel-forming and pagoda-like BMNs. A) (i) Schematic of the mechanism of the hydrogel-forming adhesive patch that contains a microneedle patch-based swellable and sticky shell and a silk fibroin-based non-swellable core. (ii) Representative photographs showing the healing of rat skin wounds and (iii) breaking strength of wounds after the different treatments. Statistical significance is designated $*p < 0.05$. Reprinted from ⁴³ with permission from Elsevier. MAP: mussel adhesive protein, HA: hyaluronic acid, SL: single-layered, DL: double-layered. **B)** Design and hemostatic function of the bioinspired pagoda-like BMN patches. (i) Schematic of the sting of a wasp. (ii) Schematic of the multi-layer microneedle patch with dodecyl-modified chitosan coating. (iii) Optical images of the

multi-layer BMN patch and a single microneedle. Scale bars: 1 mm and 300 μm (inset). (iv) Schematic of the process and mechanism of liver bleeding treatment. (v) Digital images showing the detachment of the triple-layer microneedle patch and the pig liver tissue. Reprinted from⁵⁰ with permission from Elsevier.

A second study using endoparasite-inspired BMNs was targeted at improving adhesion strength to enhance wound healing, without the risk of trauma or infection associated with wound stapling and the use of chemical-based adhesives.¹⁴ Similar to the previous study,⁴³ the BMNs in this study consisted of a swellable tip to facilitate mechanical interlocking with tissue. The swellable tip was used to encapsulate a non-swellable core. The BMNs were cone-shaped to minimize the force required for tissue penetration. The study examined retention of the BMNs in intestinal tissue and for its use in skin grafts. When compared with stapled skin grafts, the endoparasite-inspired BMNs had a greater surface contact area between the skin and tissue-like hydrogel. There was stronger retention during "pull-out" tests (0.93, 0.28, 0.22 N/cm² for the BMN, stapled skin grafts, and non-stapled skin grafts, respectively). Unlike the stapled skin graft that created large holes that permitted bacteria infiltration after fixation to the skin, the BMN patches effectively prevented bacteria infiltration through tight sealing of the punctured holes via their swollen shell and non-permeable backing layer. When compared with the use of non-swellable microneedles for intestinal tissue adhesion, the BMNs exhibited greater adhesive strength (3.83 N/cm² compared to 0.48 N/cm² in the non-swellable microneedle group) and less breakage of the needles. The authors concluded that such improvement in tissue adhesion, regardless of surface chemistry, would be ideal for reducing trauma and infection risks throughout the wound healing process, with the potential also to deliver bioactive therapeutics.

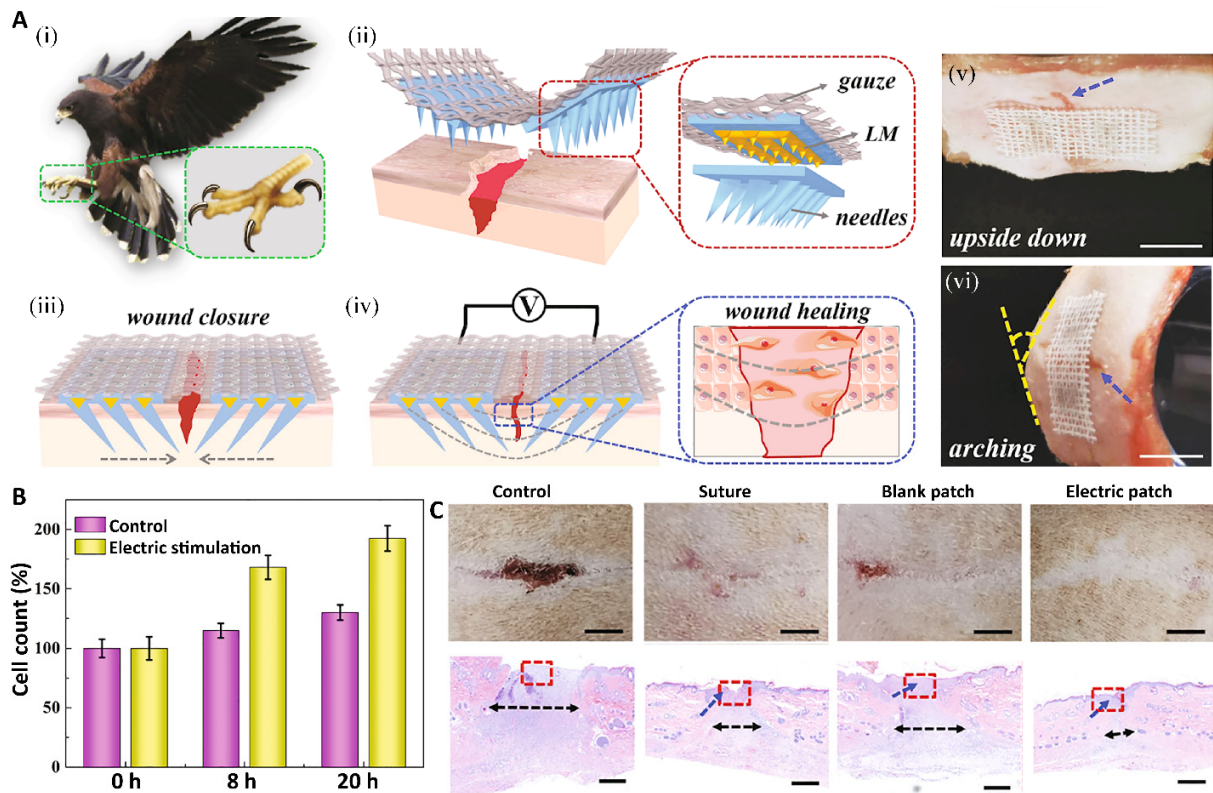


Figure 10. Eagle claw-inspired BMNs. **A)** Illustration of the claw-inspired BMN patch with liquid metal (LM) encapsulation and its application in wound healing. (i) The hallux and talons from the claw of an eagle. (ii) Composition, structure and application of the eagle claw-inspired BMN patches. (iii) Schematic of the BMN patch showing tightening of the wounded area and prevention of wound dehiscence. (iv) Schematic of the mechanism of wound healing when the BMN was connected to an external power source. (v-vi) Adhesion capability of the BMNs. Optical image of the BMNs patch after it was applied to wounded rat skin. The BMN patch remained adhered to the skin and tightened the wounded region even when the skin was placed upside down (v) and when the wound was bent (vi). Scale bars = 1 cm. **B)** Cell behaviors in response to external electric field. The number of cells within one millimeter from the copper sheets without or with electric stimulation. **C)** *In vivo* evaluation of the microneedle patch on linear wound healing. Reprinted from ⁸ with permission from Elsevier.

Microneedles are emerging armamentaria for closure of linear wounds.^{43,133–135} Inspired by the hallux and talons of the eagle’s claw that are oriented toward each other for tightly grasping its prey, a BMN patch was designed to stick to the skin and promote incisional wound healing (**Figure 10A**).⁸ The eagle claw-inspired BMN consisted of two parts that are used to hold a piece of gauze. The tips of each microneedle part were tilted so that the two parts produced a claw-like clamping structure (**Figure 8A-i, ii, iii**). Such a structure allowed the wearable BMN to fix and tighten the skin adjacent to the linear wound. This prevented the wound from dehiscence. In addition, the tips of each BMN part were connected using liquid metal encapsulation at the base. In this way, the BMN was linked to an external power source to promote wound healing (**Figure 10A-iv**) through

a variety of mechanisms that include stimulation of cell migration, simulation of endogenous wound-healing mechanisms and enhancement of cell metabolism, proliferation and differentiation.⁸ The BMN patch successfully adhered to the wounded rat skin and remained in place as the animal turned. The patch remained stable during bending, pulling and rinsing of the application site (**Figure 10A-v, vi**).⁸ The patch was also stable after immersion in phosphate-buffered saline for 24 h. A 2V/cm electrical field was generated *in vivo* by the W-shaped BMN patch to promote wound healing. **Figure 10B** shows the cell behavior in response to an external electric field. After treatment for 7 days, the rats of the suture group, blank patch group (no electrical field) and the electric patch group were all found to have faster healing times than the control (no BMN application). Furthermore, the wound width of the electric patch group was ~12 times less than the control. Epidermal thickness was ~19 times more than the control (**Figure 10C**). These encouraging results are illustrative of the positive wound healing effects of the claw-inspired BMN patch. There was also a larger mass of collagen present in the electric patch group, and much lower levels of TNF- α (indicative of inflammation) and CD68 (inflammatory cell marker) compared to the other treated groups.⁸

Honeybees utilize microscopic backward-facing barbs on their stingers to mechanically interlock its barbs with host tissue¹³⁶ These stingers exhibit an adhesion force that is 70 times stronger than a barbless acupuncture needle with interlocking mechanics.^{137,138} Inspired by these stingers, a BMN patch with backward-facing curved barbs was constructed for enhanced tissue adhesion.¹² A digital light processing 3D printing technique was used to fabricate the BMNs. The shape of the barbs was imperative in controlling tissue adhesion. A custom-built mechanical testing system was used to evaluate the adhesion performance of the BMNs, which consisted of two phases: "penetration" and "pull-out". In the penetration phase, the BMNs punctured an agarose gel or a chicken muscle tissue for a duration of 60 s. They were then removed by tensile force in the pull-out phase. In the study, the adhesion performance of a MN was defined as the maximum pull-out force required to successfully remove the BMNs from the tissue models. The number of barbs and the number of barb rows were altered to maximize tissue adhesion. As the number of barbs and the number of barb rows increased, the maximum pull-out force increased. A maximum pull-out force per needle of 0.054 N was realized from the BMN with five rows of barbs. The pull-out force represented ~18 times the maximum pull-out force of barbless microneedles. The penetration force in the barbed version was also increased by 3.6 times. The optimized needle was

further tested on chicken muscle tissue as a model of fibrous tissue. The maximum pull-out force per needle was found to be 0.176 N, approximately four times higher than that of the barbless microneedles. All the barbs remained intact and could be removed from the tissue. The strong tissue adhesive performance of the backward-facing barb-inspired BMNs will open many opportunities for diverse biomedical applications including tissue engineering, transdermal drug delivery and biosensing.

Excellent adhesion was achieved during wound healing via BMNs that mimicked the structural design of shark's teeth (**Figure 11A**).¹³⁹ A shark tooth-inspired MN with microfluidic channels can analyze the biomarkers within the wound area (**Figure 11B**). In addition, incorporating photonic crystal within MN patches boost the biochemical sensitivity and storage capacity of therapeutic agents. The use of an *N*-isopropylacrylamide thermo-responsive hydrogel enables smart drug release from the MN patch. Increasing the temperature of the infection area up to 39.4 °C leads to the shrinkage of the thermoresponsive hydrogel, thereby releasing the therapeutic drugs. As shown in **Figure 11**, flexible electrocircuits were incorporated on the microneedles to monitor the motion of wound area. Resistance was changed as bending of the finger occurs. Moreover, resistance recording of the system during breathing and swallowing indicated excellent motion sensing capability. *In vivo* examination of strip and circular-shaped wounds demonstrated a higher wound recovery rate when compared to the blank and control (**Figure 11D**).¹³⁹ Such multifunctional systems are promising in providing controlled drug release as well as wound site management.

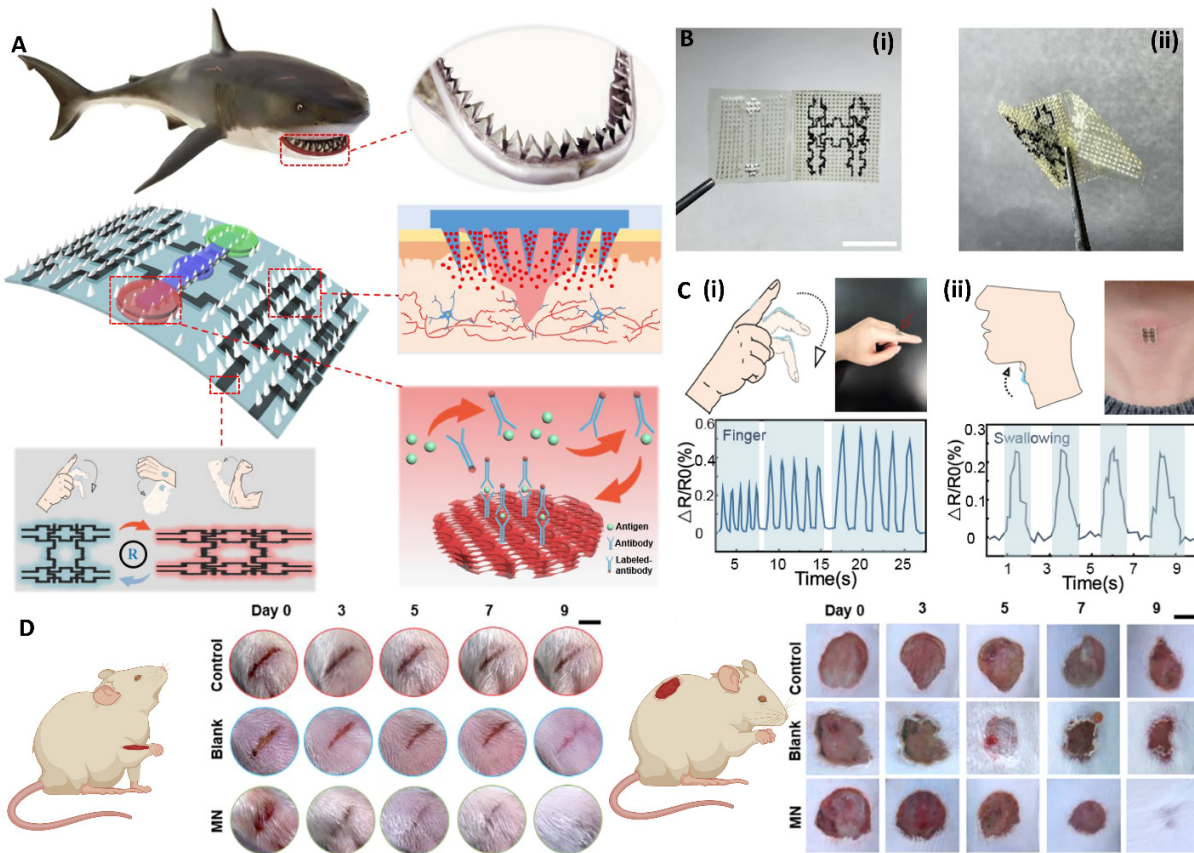


Figure 11. Shark teeth-inspired microneedles. **A)** Schematic of shark teeth-inspired microneedle dressing for intelligent wound management including motion sensing, biochemical analysis and improved healing. **B)** Image of the microneedle dressing before being folded (i) and during folding (ii). **C)** Motion sensing on the microneedle dressing. Motion sensing of bending a finger (i), and sensing of swallowing (ii). **D)** Respective images of strip-shaped wounds cut on the foot and back of a diabetic mouse that were subjected to different treatment. Reprinted from ¹³⁹ with permission from American Chemical Society.

4.3. Biopsy sampling and biosensing

Needle biopsy is used for obtaining a tissue sample for analysis.¹⁴⁰ Accurate needle insertion to the targeted site is an important aspect of cancer diagnosis. Clinically, the most severe limitation for precision needle biopsy is tissue deformation and displacement during needle insertion.^{141,142} Recently, the mosquito proboscis was used as a biomimetic model to fabricate painless BMNs for biopsy sampling (**Figure 12A-i**).¹⁴³ The mosquito proboscis plays an important role in blood suction. It is a sophisticated microneedle system that consists of a gutter-like labium that encloses a fascicle. There are two lobes (labella) at the tip of the labium. The fascicle contains six stylets: a pair of teeth-bearing maxillae, a pair of mandibles, a hypopharynx with its salivary canal and a labrum that carried sense organs on its tip. The cooperative motion of the hollow labium and the

jagged-edged maxillae reduces puncture resistance and facilitates needle insertion. This synergetic mechanism of action functions effectively to collect blood from capillary vessels with no bleeding or pain (**Figure 12A-ii**).^{13,144}

Inspired by this sophisticated natural suction mechanism, a three-piece BMN imitating the mosquito's proboscis (one labrum and a pair of maxillae) was constructed (**Figure 12A-iii**). This design was robust enough to be inserted easily into an artificial skin without buckling.¹³ The resistance force during puncturing of the BMN into artificial skin derived from polydimethylsiloxane was the highest when the needles were not vibrating, lower when both halves of the needles vibrated and the lowest when each half of the needles vibrated alternatively. The BMNs successfully collected blood at a rate of 0.025 µL/s using capillary force (0.3 µL is required for blood glucose measurement, which would take 12 s with the use of the BMNs).¹³ Both the harpoon-shaped notches at the needle tip and the reciprocating needle cannula vibrate during microneedle insertion. The mosquito proboscis-inspired BMN and a traditional direct needle insertion strategy were compared for local tissue deformation and global prostate displacement by optically tracking the displacement of particle-embedded tissue-mimicking phantoms. The mosquito proboscis-inspired BMNs reduced both local tissue deformation and global prostate displacement when compared to direct or incremental insertion of the needle cannula.¹⁴³ This encouraging result was thought to be attributed to the opposing movement of the needle cannula of the mosquito-inspired BMNs, as well as the notches that stabilized and reduced tissue deformation during needle insertion.

Although the proof-of-concept study was successful, further studies are required to identify the effects of altering parameters such as notch shape, width and angle. This should aid determine the optimal needle design that produces the minimal insertion force while maximizing tissue anchoring. Such a state-of-the-art BMN, if successful, will enable diabetic patients to collect their blood for the glucose level measurement painlessly and with minimal bleeding.^{4,145,146}

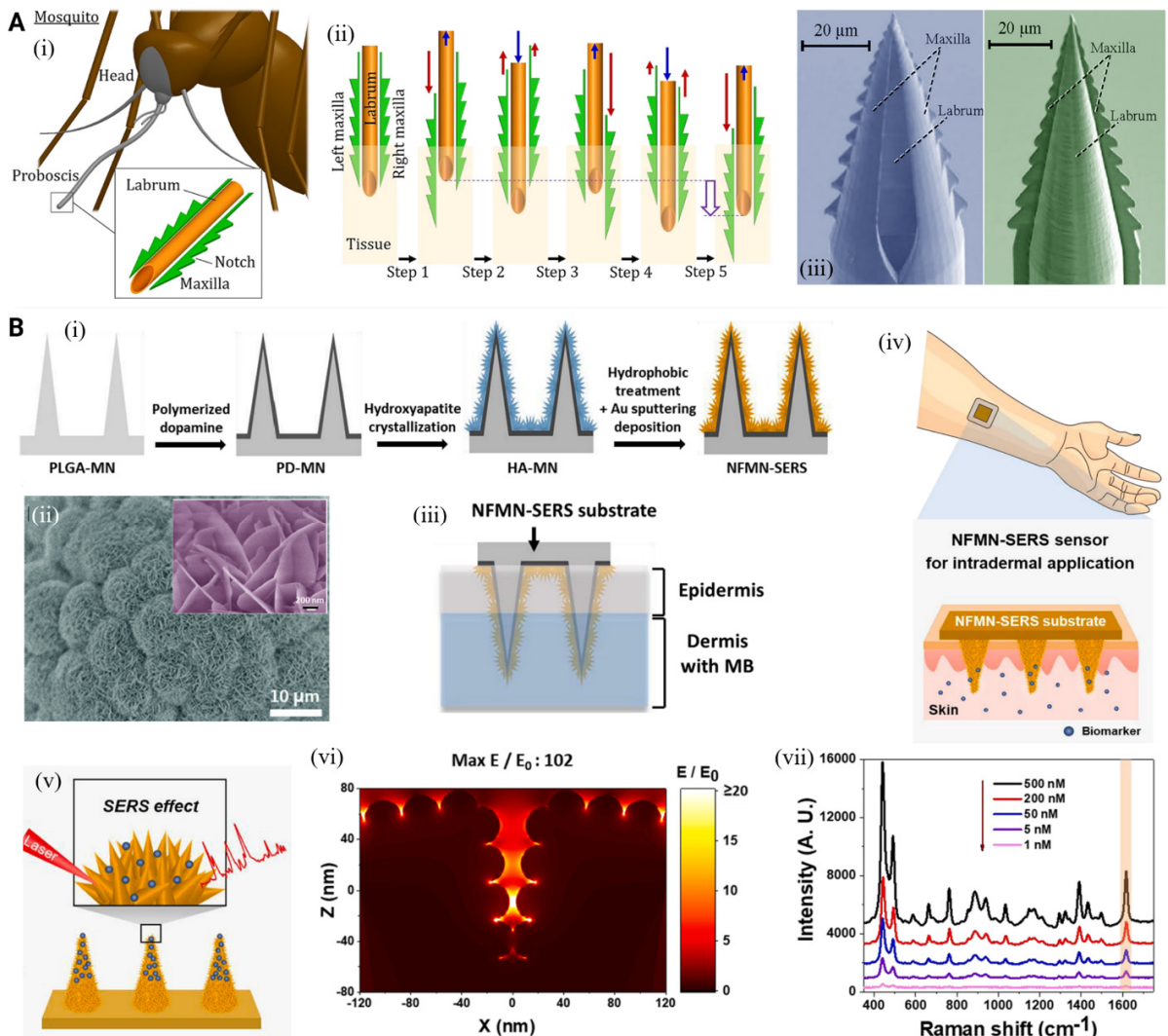


Figure 12. Bioinspired microneedle patches for biopsy sampling and biosensing applications. **A)** Mosquito-inspired BMN patches for biosensing applications. (i) Mosquito proboscis has one labrum and two maxillae. (ii) Incremental motion during insertion of the proboscis reduces surrounding tissue deformation and insertion force. Reprinted from ¹⁴³ with permission from Nature. (iii) SEM images of BMNs made of IP-Dip polymer; front view (left) and back view (right). Reprinted from ¹⁰⁸ under open access license. **(B)** Nanoflower-inspired BMN patches for biosensing applications. (i) Schematic of the preparation of the NFMN-SERS substrate. (ii) SEM images of HA-coated BMN patch at different magnifications. (iii) Scheme illustrating the insertion of a NFMN-SERS patch into the two-layered skin phantom. (iv-v) Schematic of intradermal application of the NFMN-SERS sensor. Inset in (v) represents the flower-like nanosystem formed on the BMNs. (vi) Finite-difference time-domain simulations of the electromagnetic field enhancement of Au nanoislands on the intersecting petals at a facing angle of 15°. (vii) Detection of MB applied at different concentrations to the phantom dermis by SERS. PD: polydopamine; HA: hydroxyapatite; NFMN: Au-nanoflower on microneedle; SERS: surface-enhanced Raman scattering; MB: methylene blue. Reprinted from ¹¹⁶ with permission from Elsevier.

Skin interstitial fluid contains different biomarkers that range from small molecules to proteins.¹⁴⁷ These biomarkers reflect the physiological function of organisms. Accordingly, accurate detection of these interstitial fluid-residing molecules using non-invasive and facile sampling is highly desirable.¹⁴⁸ Despite advances in the biosensing arena, blood samples are still collected by conventional syringes/needles.¹⁴⁹ This blood drawing method relies on venous blood withdrawal or finger-pricking, trained staff and access to laboratory facilities. Hence, new diagnostic methods that rely on interstitial fluid biomarker detection have been developed. These methods include the use of microchips^{150–152} and microneedle arrays^{153,154}.

Because of the ability of microneedle patches to penetrate skin without contacting capillaries and nerve fibers, these microdevices may be used to extract biomarkers of interstitial fluid for subsequent *ex vivo* measurements.^{149,153–155} Jung *et al.*¹¹⁶ fabricated a biocompatible nanoflower-like BMN sensor with high sensitivity and signal uniformity for intradermal biosensing applications (**Figure 12Bi-vii**). The sensor was based on surface-enhanced Raman spectroscopy (SERS), a potent technique used for the identification of molecules.¹⁵⁶ Gold nanoislands were deposited on the petals of the flower-like hydroxyapatite layer to generate hot spots for SERS. The origin of the SERS effect and plasmonic coupling between the petals formed with Au nanoislands were investigated by finite-difference time-domain simulation of electromagnetic field distribution for the NFMN-SERS substrate. It was found that petals adjacent to the nanoflower structure created enhanced plasmonic coupling effect for sensitivity improvement.¹¹⁶ Although no *in vivo* study was performed, these novel BMN patches pave a new direction for point-of-care diagnostics, minimally-invasive sampling and analysis of biomarkers in the interstitial fluid.

4.4. Optimization of mechanical strength and skin penetration

4.4.1. Solid microneedles

As skin is inherently elastic, microneedles must be able to overcome this elasticity for successful penetration. To enhance the mechanical properties of microneedle patches for improved penetration, nature-inspired designs were employed. For instance, frozen microneedles inspired by naturally-occurring ice were designed to address the demands of microneedles implantation (**Figure 13A**).¹⁵⁷ During the insertion process, the backing part slowly melted, with their tips detaching from the base and left in the skin for sustained drug release. Several types of materials,

including water, Matrigel, methacrylated gelatin and alginate, were evaluated to compare the mechanical strengths of the microneedles before and after freezing. Unfrozen microneedles prepared methacrylated gelatin and alginate were incapable of being thoroughly released from the mold, while water and Matrigel could not even create the shape of the needles. In contrast, all frozen materials could completely be released from the mold with an intact microneedle shape. When the implantation capability of different microneedles was examined,¹⁵⁷ unfrozen microneedles could barely perforate the model skin. In contrast, all frozen microneedles completely punctured both agarose and porcine skin. The strength of all water-containing microneedles was remarkably increased in the frozen state (**Figure 13B and C**). *In vivo* evaluation identified no serious fungal infection for the ketoconazole group (an antifungal drug) and the BMN group, when compared with the control group and the MN group (**Figure 13D and E**).¹⁵⁷

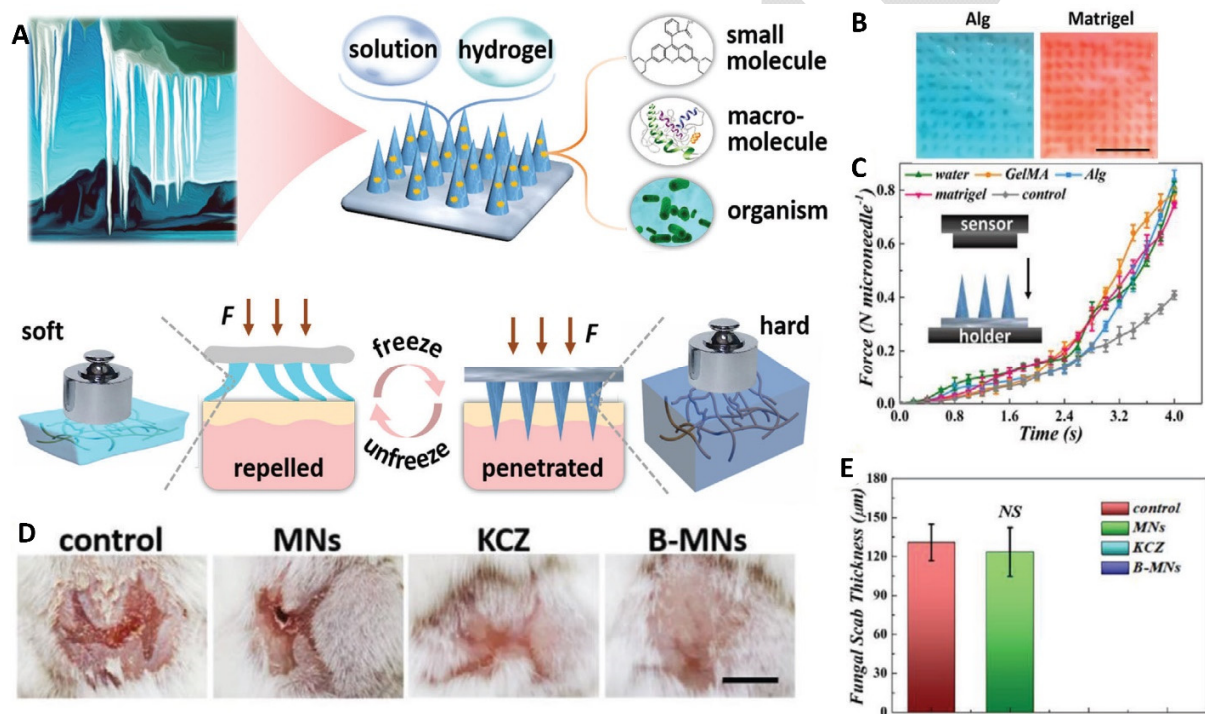


Figure 13. Ice-inspired MNs for improving skin penetration. (A) Schematic of the composition and properties of the ice-inspired MNs that transform from soft materials to hard materials. (B) Digital images of porcine skin after penetration of alginate and Matrigel. (C) Compressive forces of four kinds of ice microneedles and the poly(ethylene glycol) diacrylate control. Representative photos of the back skins of mice in the control group, the MNs group, the ketoconazole (KCZ) group, and the BMNs group on day 13. (E) Quantitative analysis of the fungal scab thicknesses of the mice. Reprinted from ¹⁵⁷ under CC-BY license.

The teeth of limpets exhibit strong mechanical properties. This is attributed to their unique hierarchical structure, in which abundant goethite nanofibers are arranged parallel to the surface (**Figure 14A-i**)¹⁵⁸. The shelled aquatic snails can adhesive strongly to rocks.¹⁵⁸ Limpet tooth-inspired BMNs were fabricated using magnetic field-assisted 3D printing to enhance the mechanical strength of the microneedles (**Figure 14A-ii, iii, iv, v**).¹¹ The 3D-printed BMNs had precise micro-filler alignment, with aligned nanoparticle bundles incorporated inside the microneedles. Compared to 3D-printed hierarchical structures with random iron oxide nanoparticles, structured loaded with aligned iron oxide NPs showed higher mechanical properties. This endowed each layer with maximum performance. As shown in **Figure 14A-vi**, elastic buckling occurred on a polymer-based microneedle when a compression load was applied. Physical compression testing indicated that the compressive modulus of 2.5 wt% iron oxide NPs-based composite BMN was 1.79 times and 4 times that of the iron oxide NPs -based composite and the pure polymer, respectively. The 2.5% aIOs composite BMN could pierce an artificial skin without buckling. In contrast, microneedles prepared from the pure polymer buckled during insertion. In subsequent *ex vivo* studies, insertion of the aIO-containing BMNs into porcine skin was confirmed using hematoxylin and eosin staining.¹¹ A murine model was also used to investigate "pain-like" behavior. In that experiment, one group of mice wore the magnetic field-assisted 3D printed BMN patch while the other group had no patch. There was no pain-associated behavioral changes, including restlessness, self-isolation, aggression and rapid breathing during long-term observation of the mice wearing the BMN patch.¹¹ An *in vitro* release study using rhodamine B-coated magnetic field-assisted 3D-printed BMNs demonstrated burst release of the cargo dye in the first hour. The remaining rhodamine B fluorescent dye (50%) was gradually released from the BMNs over the course of two days. (**Figure 14A-viii**). Another *in vivo* study showed that the magnetic field-assisted 3D-printed BMNs containing aIOs could be painlessly inserted into porcine skin with controllable drug release. This study exquisitely illustrated how the geometrical morphology of microneedles may be altered through biomimetic approaches to overcome the suboptimal mechanical properties of conventional microneedles.¹²⁴

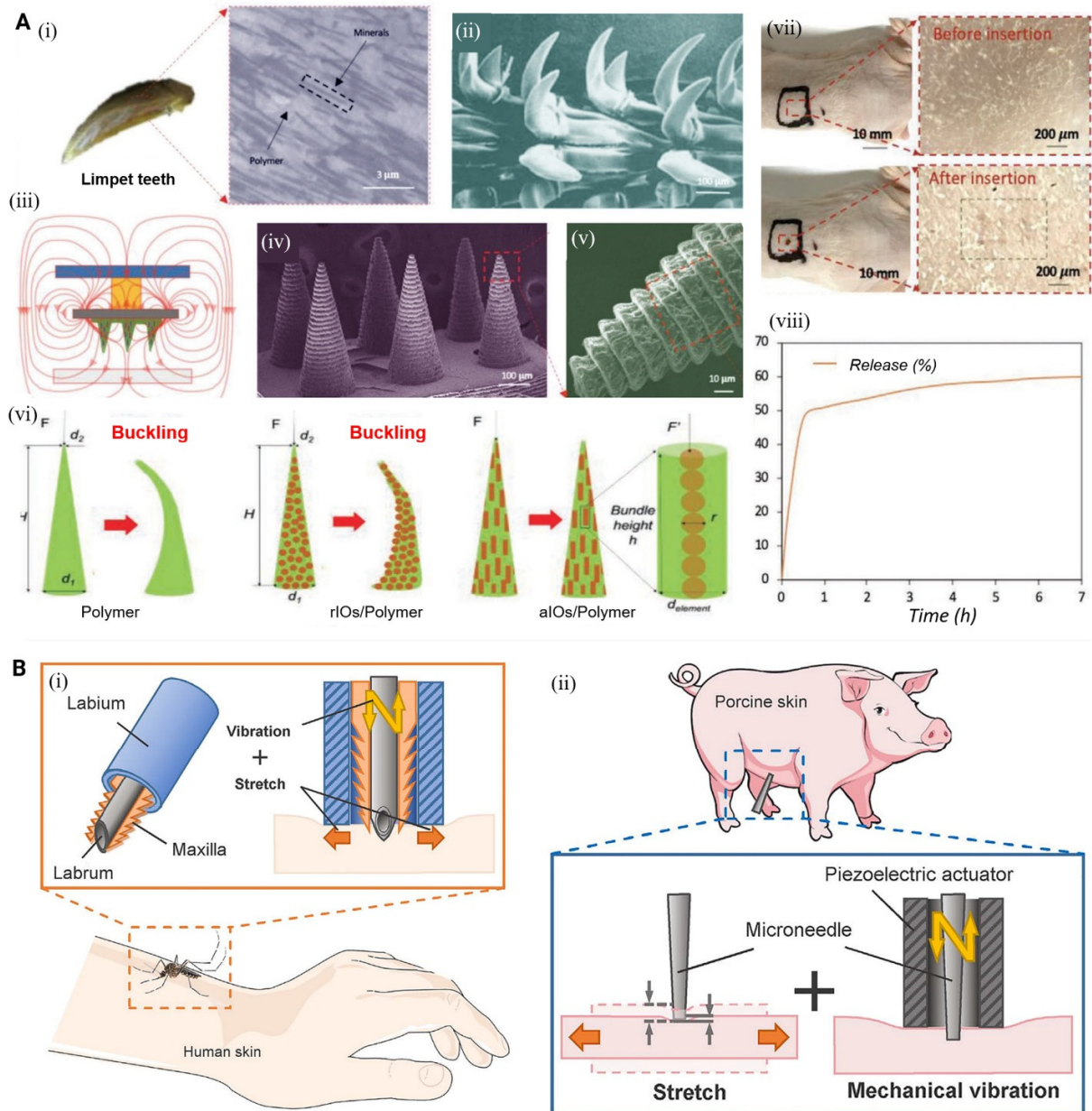


Figure 13. Limpet tooth-inspired and mosquito-inspired microneedle patches for improved mechanical strength. A) (i) Optical image and cross-sectional view of a limpet tooth with aligned mineral nanofibers. (ii) High magnification view of limpet teeth. (iii) Schematic of limpet tooth-inspired BMN using magnetic field-assisted 3D printing. (iv) SEM images of magnetic field-assisted 3D-printed microneedle array. (v) High magnification of one 3D-printed BMN array with aligned iron oxide nanoparticles (aIOs). (vi) Schematic of shape deformation of the BMNs with pure polymer, random iron oxide nanoparticles (rIOs) and aIOs when a compression load is applied. (vii) Optical microscopy images of mouse skin before and after the insertion of the BMNs, showing small holes in the skin after insertion of the BMNs. (viii) Cumulative release of rhodamine-B from magnetic field-assisted 3D-printed microneedles coated with rhodamine-B over time. Reprinted from ¹¹ with permission from Wiley. B) (i) Insertion of a mosquito proboscis into human skin by pressing down the labium and vibrating the maxillae (i.e. two harpoon-shape

notched-maxillae and center labrum). (ii) Microneedle insertion using mechanophysical stimulus. © Elsevier.

4.4.2. Hollow microneedles

Besides of solid-based patches, other types of microneedles, e.g., hollow, have been optimized to augment the penetration. For instance, the effects of stretch and mechanical vibration on the insertion of BMNs as well as the biological mechanisms of mosquito- and honeybee-inspired BMNs were investigated.¹⁵⁹ The researchers discovered that the advanced skin-piercing mechanisms exhibited by the BMNs indicated that skin resistance to the insertion of the needle-like objects was affected by mechanophysical stimulus (**Figure 14B**). They found that the application of a dynamic mechanophysical stimulus controlled the value and changes in skin resistance to microneedle insertion. By simulating the proboscis of a mosquito, the application of mechanophysical stimulus enabled a microneedle patch to be easily and deeply inserted into the skin in a controlled manner (**Figure 14B**).¹⁵⁹ Such hollow MN patches can be employed for extraction of interstitial fluid for biosensing application, or for delivering special therapeutics such as plasma gas for cancer immunotherapy.¹⁶⁰

5. Challenges and future perspectives

Bioinspired microneedle systems represent an innovative technology that are potentially useful for biomedical applications. Spurred by the advances of micro/nano fabrication technologies, materials science and engineering and biotechnologies, many BMNs with sophisticated designs have been realized. This review summarizes the design rationale, fabrication techniques and representative biomedical applications of BMNs.

From fabrication and marketability point of view, the lack of available technology for large-scale production is the major problem to overcome for the commercialization of BMNs. This issue is the Achilles' heel of most published BMN-based investigations. Materials selection, preparation methods/conditions, compatibility with manufacturing procedures, as well as the potential for industrial scale-up should be considered in future studies.³⁹ Standardization of the microneedle manufacturing processes is necessary so that the construction of different microneedles may be realized with minimal modifications. One option is to perform an additive manufacturing process in which the materials employed for synthesis can change while the same assembly protocol is maintained for different applications. Replica molding approach is an interesting approach for

scalable BMN production. Nevertheless, complicated architectures (e.g. microneedles with barbs inspired by the honeybee) are difficult to be fabricated even with “standard” 3D printers (static printing). In most cases, they are almost impossible to be reproduced by replica molding approaches. This issue may be potentially addressed by the development of 4D printing technology, in which materials with preprogrammed geometry or functionality are triggered by external stimuli. Accordingly, 4D and dynamic printing enable the fabrication of complicated BMN arrays. This contemporary technology benefits from an architecture that may be triggered by external or internal stimuli, leading to the construction of multifaceted unprintable geometries by means of post-printing stimulation.

In the authors’ opinion, one of the most promising approaches in the development of BMNs is the direct laser writing (DLW) approach. This technique uses two-photon polymerization via near-infrared radiation.¹⁶¹ Compared with conventional microneedle fabrication technologies DLW possess intrinsically higher resolution, and allows the fabrication highly complex morphology and architecture, including re-entrant angles and micro-nano features exploiting anisotropic friction, interlocking and anchoring. Progress in increasing writing speed may soon lead to sustainable fabrication speed. Considering that research on materials for two-photon lithography is very active, more biocompatible, biodegradable and tailorabile materials may soon be available for this use.¹⁶¹ Given the versatility of the technology in generating 3D structures with submicron resolution and the emerging of new functional materials,¹⁶¹ complex BMNs for online diagnosis and advanced treatments may be realized in the not-so-distant future. Combining the accuracy of LDW fabrication with 4D functional materials approach, it will make possible in future the fabrication of BMN with embedded integrated electronic capability, and the selective surface functionalization, toward the implementation of advanced “lab-on-a-needle” systems for advanced sensing and close loop drug release.

Bioinspired microneedle technology holds tremendous promise for many biomedical applications. Examples include the use of mechanically-interlocked BMN for sustained drug delivery, and acceleration of incisional wound healing wiith sticky BMN patches. In addition, construction of BMNs with specific architecture and superior mechanical property prevent them from falling off the skin. Despite all the efforts that have been comtemplated to date, such platforms are still in an immature phase of development and many challenges exist that should be addressed prior to their commercialization.

First, the success of BMNs relies profoundly on the rational design of microneedles with long-term biocompatibility and biodegradability.¹⁶² Prolonged treatment with BMN systems requires that these systems are biocompatible. Animal studies should be performed to evaluate the biosafety concerns upon the usage of BMNs. To augment the potential clinical applications of BMNs, safety concerns from the perspectives of composition, drug toxicity as well as physical contact with healthy and wound tissues should be taken into account at the early stage of development.¹⁶²

There is no reported application of BMNs on anti-cancer therapy. As an emerging delivery device, BMN patches may be utilized to deliver anti-cancer agents including chemotherapeutics, genetic materials, immunotherapeutics, photothermal and/or photodynamic agents for combating cancer efficiently and with minimal invasiveness (**Figure 14**).^{4,163-166} In addition, the design and construction of closed-loop drug delivery systems via the use BMNs is still unavailable.¹⁶⁷ These emerging smart devices have the capability to increase therapy efficacy and reduce side effects during drug administration. In the future, smart BMN patches are anticipated to function as biosensors for diabetes management, antibiotic concentration gauging and auto-anticoagulation regulation.¹⁶⁸

In recent years, rather than skin, other tissue and organ were targeted by MNs. Microneedles have the potential for new therapeutic applications such as the treatment of eye diseases,¹⁶⁹ neuropathic pain,¹⁷⁰ autoimmune disorders⁴, heart diseases,¹⁷¹ hair loss,¹⁷² and obesity^{173,174}. Langer *et al.*¹⁷⁵ successfully delivered 1 mg of human growth hormone and human insulin to the oral cavity of a pig using macromolecules-loaded microneedle patches within 30 s. This amazing achievement opens new vistas for painless delivery of biological molecules and drugs via the oral cavity.¹⁷⁵ In another study, Zhao *et al.*¹⁷⁶ developed Lego-brick-stacking-inspired BMNs with magnetically-responsive behavior via a multistage 3D fabrication strategy. The MN was stable in the presence of gastric secretions through their encapsulation into a commercial enteric capsule.¹⁷⁶ Similarly, bioinspired MN can be employed for the aforementioned tissues and organs. Accordingly, because of the stronger mechanical properties and mechanically interlocking of BMN patches compared with conventional microneedle patches, nature-mimicking MNs offer superior solutions in the biomedical field.

Acknowledgments

P.M. and V.M. are grateful for funding received from the European Horizon 2020 Research and Innovation Programme under Grant Agreement No 899349 (5D NanoPrinting). G.C. is supported by the startup funds from McGill University.

Declaration of interests

The authors declare no conflict of interest.

References

1. Jamaledin, R. *et al.* (2020). Advances in Antimicrobial Microneedle Patches for Combating Infections. *Adv. Mater.* *32*, 2002129.
2. Makvandi, P. *et al.* (2021). Stimuli-responsive transdermal microneedle patches. *Mater. Today* *47*, 206–222.
3. Jamaledin, R. *et al.* (2020). Progress in Microneedle-Mediated Protein Delivery. *J. Clin. Med.* *9*, 542.
4. Amani, H. *et al.* (2021). Microneedles for painless transdermal immunotherapeutic applications. *J. Control. Release* *330*, 185–217.
5. Jamaledin, R. *et al.* (2020). Engineered Microneedle Patches for Controlled Release of Active Compounds: Recent Advances in Release Profile Tuning. *Adv. Ther.* *3*, 2000171.
6. Makvandi, P. *et al.* (2021). Engineering Microneedle Patches for Improved Penetration: Analysis, Skin Models and Factors Affecting Needle Insertion. *Nano-Micro Lett.* *13*, 93.
7. Bae, W.-G. *et al.* (2019). Snake fang-inspired stamping patch for transdermal delivery of liquid formulations. *Sci. Transl. Med.* *11*, eaaw3329.
8. Zhang, X. *et al.* (2021). Claw-inspired microneedle patches with liquid metal encapsulation for accelerating incisional wound healing. *Chem. Eng. J.* *406*, 126741.
9. Oka, K. *et al.* (2002). Fabrication of a micro needle for a trace blood test. *Sensors Actuators, A Phys.* *97–98*, 478–485.
10. Bhushan, B. (2009). Biomimetics: lessons from nature—an overview. *Philos. Trans. R. Soc. A Math. Phys. Eng. Sci.* *367*, 1445–1486.
11. Li, X. *et al.* (2021). Limpet Tooth-Inspired Painless Microneedles Fabricated by Magnetic Field-Assisted 3D Printing. *Adv. Funct. Mater.* *31*, 2003725.
12. Han, D. *et al.* (2020). 4D Printing of a Bioinspired Microneedle Array with Backward-Facing Barbs for Enhanced Tissue Adhesion. *Adv. Funct. Mater.* *30*, 1909197.
13. Suzuki, M., Takahashi, T. & Aoyagi, S. (2018). 3D laser lithographic fabrication of hollow microneedle mimicking mosquitos and its characterisation. *Int. J. Nanotechnol.* *15*, 157–173.

14. Yang, S. Y. *et al.* (2013). A bio-inspired swellable microneedle adhesive for mechanical interlocking with tissue. *Nat. Commun.* *4*, 1–10.
15. Holmes, R. (2016). *The origin of species. Economist (United Kingdom)* vol. 412 (PF Collier & son New York, 2016).
16. Libonati, F. & Buehler, M. J. (2017). Advanced Structural Materials by Bioinspiration. *Adv. Eng. Mater.* *19*, 1600787.
17. Lossada, F., Hoenders, D., Guo, J., Jiao, D. & Walther, A. (2020). Self-Assembled Bioinspired Nanocomposites. *Acc. Chem. Res.* *53*, 2622–2635.
18. Zhang, B. *et al.* (2020). Advanced bio-inspired structural materials: Local properties determine overall performance. *Mater. Today* *41*, 177–199.
19. Finnemore, A. *et al.* (2012). Biomimetic layer-by-layer assembly of artificial nacre. *Nat. Commun.* *3*, 1–6.
20. Wegst, U. G. K., Bai, H., Saiz, E., Tomsia, A. P. & Ritchie, R. O. (2015). Bioinspired structural materials. *Nat. Mater.* *14*, 23–36.
21. Raut, H. K. *et al.* (2020). Tough and Strong: Cross-Lamella Design Imparts Multifunctionality to Biomimetic Nacre. *ACS Nano* *14*, 9771–9779.
22. Han, Z., Feng, X., Guo, Z., Niu, S. & Ren, L. (2018). Flourishing Bioinspired Antifogging Materials with Superwettability: Progresses and Challenges. *Adv. Mater.* *30*, 1704652.
23. Rawat, P., Zhu, D., Rahman, M. Z. & Barthelat, F. (2021). Structural and mechanical properties of fish scales for the bio-inspired design of flexible body armors: A review. *Acta Biomater.* *121*, 41–67.
24. Wang, X. *et al.* (2021). Beetle and cactus-inspired surface endows continuous and directional droplet jumping for efficient water harvesting. *J. Mater. Chem. A* *9*, 1507–1516.
25. Wu, P., Wang, J. & Jiang, L. (2020). Bio-inspired photonic crystal patterns. *Mater. Horizons* *7*, 338–365.
26. Potyrailo, R. A. *et al.* (2015). Towards outperforming conventional sensor arrays with fabricated individual photonic vapour sensors inspired by Morpho butterflies. *Nat. Commun.* *6*, 1–12.
27. Chen, Y. *et al.* (2020). Mussel-inspired sandwich-like nanofibers/hydrogel composite with super adhesive, sustained drug release and anti-infection capacity. *Chem. Eng. J.* *399*, 125668.
28. Liu, K., Du, J., Wu, J. & Jiang, L. (2012). Superhydrophobic gecko feet with high adhesive forces towards water and their bio-inspired materials. *Nanoscale* *4*, 768–772.
29. Chen, H. *et al.* (2018). Ultrafast water harvesting and transport in hierarchical microchannels. *Nat. Mater.* *17*, 935–942.
30. Liu, M., Wang, S. & Jiang, L. (2017). Nature-inspired superwettability systems. *Nat. Rev. Mater.* *2*, 1–17.

31. Zhong, H. *et al.* (2020). Reusable and Recyclable Graphene Masks with Outstanding Superhydrophobic and Photothermal Performances. *ACS Nano* *14*, 6213–6221.
32. Li, K. *et al.* (2013). Structured cone arrays for continuous and effective collection of micron-sized oil droplets from water. *Nat. Commun.* *4*, 1–7.
33. Yang, Y. *et al.* (2019). Electrically assisted 3D printing of nacre-inspired structures with self-sensing capability. *Sci. Adv.* *5*, eaau9490.
34. Fiorello, I. *et al.* (2020). Climbing Plant-Inspired Micropatterned Devices for Reversible Attachment. *Adv. Funct. Mater.* *30*, 2003380.
35. Liu, K. & Jiang, L. (2011). Bio-inspired design of multiscale structures for function integration. *Nano Today* *6*, 155–175.
36. Lee, H., Lee, B. P. & Messersmith, P. B. (2007). A reversible wet/dry adhesive inspired by mussels and geckos. *Nature* *448*, 338–341.
37. Bao, Z., Gao, M., Sun, Y., Nian, R. & Xian, M. (2020). The recent progress of tissue adhesives in design strategies, adhesive mechanism and applications. *Mater. Sci. Eng. C* *111*, 110796.
38. Izumi, H., Suzuki, M., Aoyagi, S. & Kanzaki, T. (2011). Realistic imitation of mosquito's proboscis: Electrochemically etched sharp and jagged needles and their cooperative inserting motion. *Sensors Actuators, A Phys.* *165*, 115–123.
39. Larrañeta, E., Lutton, R. E. M., Woolfson, A. D. & Donnelly, R. F. (2016). Microneedle arrays as transdermal and intradermal drug delivery systems: Materials science, manufacture and commercial development. *Mater. Sci. Eng. R Reports* *104*, 1–32.
40. Donnelly, R. F., Singh, T. R. R., Morrow, D. I. J. & Woolfson, A. D. (2012). *Microneedle-Mediated Transdermal and Intradermal Drug Delivery. Microneedle-Mediated Transdermal and Intradermal Drug Delivery* (John Wiley & Sons, Ltd, 2012). doi:10.1002/9781119959687.
41. HAMMOND, R. A. (1966). The Proboscis Mechanism of *Acanthocephalus Ranae*. *J. Exp. Biol.* *45*, 203–213.
42. Seong, K. Y. *et al.* (2017). A self-adherent, bullet-shaped microneedle patch for controlled transdermal delivery of insulin. *J. Control. Release* *265*, 48–56.
43. Jeon, E. Y. *et al.* (2019). Bio-inspired swellable hydrogel-forming double-layered adhesive microneedle protein patch for regenerative internal/external surgical closure. *Biomaterials* *222*, 119439.
44. Jeon, E. Y. *et al.* (2015). Rapidly light-activated surgical protein glue inspired by mussel adhesion and insect structural crosslinking. *Biomaterials* *67*, 11–19.
45. Fancy, D. A. & Kodadek, T. (1999). Chemistry for the analysis of protein-protein interactions: Rapid and efficient cross-linking triggered by long wavelength light. *Proc. Natl. Acad. Sci. U. S. A.* *96*, 6020–6024.
46. Hwang, D. S., Gim, Y., Yoo, H. J. & Cha, H. J. (2007). Practical recombinant hybrid mussel

- bioadhesive fp-151. *Biomaterials* 28, 3560–3568.
- 47. Hwang, D. S., Zeng, H., Lu, Q., Israelachvili, J. & Waite, J. H. (2012). Adhesion mechanism in a DOPA-deficient foot protein from green mussels. *Soft Matter* 8, 5640–5648.
 - 48. Lu, Q. *et al.* (2013). Nanomechanics of Cation- π Interactions in Aqueous Solution. *Angew. Chemie* 125, 4036–4040.
 - 49. Zhang, X., Chen, G., Yu, Y., Sun, L. & Zhao, Y. (2020). Bioinspired Adhesive and Antibacterial Microneedles for Versatile Transdermal Drug Delivery. *Research 2020*, 1–9.
 - 50. Zhang, X. *et al.* (2021). Bioinspired pagoda-like microneedle patches with strong fixation and hemostasis capabilities. *Chem. Eng. J.* 414, 128905.
 - 51. Zhang, X. *et al.* (2019). Bio-inspired clamping microneedle arrays from flexible ferrofluid-configured moldings. *Sci. Bull.* 64, 1110–1117.
 - 52. Shang, L. *et al.* (2018). Bio-Inspired Anisotropic Wettability Surfaces from Dynamic Ferrofluid Assembled Templates. *Adv. Funct. Mater.* 28, 1705802.
 - 53. Assadsangabi, B., Hashem Jayhooni, S. M., Stack, T. & Takahata, K. (2019). High-Aspect-Ratio Needle-Shaped Mold Fabrication Using Rosensweig Instability in Ferrofluids. *2019 20th Int. Conf. Solid-State Sensors, Actuators Microsystems Eurosensors XXXIII, TRANSDUCERS 2019 EUROSENSORS XXXIII* 394–397 doi:10.1109/TRANSDUCERS.2019.8808573.
 - 54. Chen, Z. *et al.* (2018). Rapid fabrication of microneedles using magnetorheological drawing lithography. *Acta Biomater.* 65, 283–291.
 - 55. Hwang, H. H., Zhu, W., Victorine, G., Lawrence, N. & Chen, S. (2018). 3D-Printing of Functional Biomedical Microdevices via Light- and Extrusion-Based Approaches. *Small Methods* 2, 1700277.
 - 56. Economidou, S. N., Lamprou, D. A. & Douroumis, D. (2018). 3D printing applications for transdermal drug delivery. *Int. J. Pharm.* 544, 415–424.
 - 57. Aimar, A., Palermo, A. & Innocenti, B. (2019). The Role of 3D Printing in Medical Applications: A State of the Art. *J. Healthc. Eng.* 2019, 5340616.
 - 58. Tang, T. O., Holmes, S., Dean, K. & Simon, G. P. (2020). Design and fabrication of transdermal drug delivery patch with milliprojections using material extrusion 3D printing. *J. Appl. Polym. Sci.* 137, 48777.
 - 59. Luzuriaga, M. A., Berry, D. R., Reagan, J. C., Smaldone, R. A. & Gassensmith, J. J. (2018). Biodegradable 3D printed polymer microneedles for transdermal drug delivery. *Lab Chip* 18, 1223–1230.
 - 60. Matsuda, T. & Mizutani, M. (2002). Liquid acrylate-endcapped biodegradable poly(ϵ -caprolactone-co-trimethylene carbonate). II. Computer-aided stereolithographic microarchitectural surface photoconstructs. *J. Biomed. Mater. Res.* 62, 395–403.
 - 61. Xenikakis, I. *et al.* (2019). Fabrication and finite element analysis of stereolithographic 3D printed microneedles for transdermal delivery of model dyes across human skin in vitro.

Eur. J. Pharm. Sci. 137, 104976.

62. Economidou, S. N. *et al.* (2019). 3D printed microneedle patches using stereolithography (SLA) for intradermal insulin delivery. Mater. Sci. Eng. C 102, 743–755.
63. Krieger, K. J. *et al.* (2019). Simple and customizable method for fabrication of high-aspect ratio microneedle molds using low-cost 3D printing. Microsystems Nanoeng. 5, 1–14.
64. Uddin, M. J. *et al.* (2020). 3D printed microneedles for anticancer therapy of skin tumours. Mater. Sci. Eng. C 107, 110248.
65. Economidou, S. N. *et al.* (2021). A novel 3D printed hollow microneedle microelectromechanical system for controlled, personalized transdermal drug delivery. Addit. Manuf. 38, 101815.
66. Wang, J., Goyanes, A., Gaisford, S. & Basit, A. W. (2016). Stereolithographic (SLA) 3D printing of oral modified-release dosage forms. Int. J. Pharm. 503, 207–212.
67. Gittard, S. D. *et al.* (2011). Deposition of antimicrobial coatings on microstereolithography-fabricated microneedles. Jom 63, 59–68.
68. Pere, C. P. P. *et al.* (2018). 3D printed microneedles for insulin skin delivery. Int. J. Pharm. 544, 425–432.
69. Farias, C. *et al.* (2018). Three-dimensional (3D) printed microneedles for microencapsulated cell extrusion. Bioengineering 5,.
70. Xu, X. *et al.* (2020). Stereolithography (SLA) 3D printing of an antihypertensive polyprintlet: Case study of an unexpected photopolymer-drug reaction. Addit. Manuf. 33, 101071.
71. Bertsch, A. & Renaud, P. (2019). Microstereolithography. in *Three-Dimensional Microfabrication Using Two-Photon Polymerization* (ed. Baldacchini, T.) 25–56 (William Andrew Publishing, 2019). doi:10.1016/B978-0-12-817827-0.00050-3.
72. Li, D. *et al.* (2019). An automated 3D visible light stereolithography platform for hydrogel-based micron-sized structures. AIP Adv. 9, 065204.
73. Miller, P. R. *et al.* (2011). Integrated carbon fiber electrodes within hollow polymer microneedles for transdermal electrochemical sensing. Biomicrofluidics 5, 13415.
74. Yao, W. *et al.* (2020). 3D Printed multi-functional hydrogel microneedles based on high-precision digital light processing. Micromachines 11,.
75. Lee, B. (2008). Introduction to 12 Degree Orthogonal Digital Micromirror Devices (DMDs). Texas Instrum. 1–13.
76. Jasveer, S. & Jianbin, X. (2018). Comparison of Different Types of 3D Printing Technologies. Int. J. Sci. Res. Publ. 8, 1–9.
77. Rogers, C. I., Qaderi, K., Woolley, A. T. & Nordin, G. P. (2015). 3D printed microfluidic devices with integrated valves. Biomicrofluidics 9, 16501.
78. Zhang, Z. chen, Li, P. lun, Chu, F. ting & Shen, G. (2019). Influence of the three-

- dimensional printing technique and printing layer thickness on model accuracy. *J. Orofac. Orthop.* *80*, 194–204.
79. Etemad-Shahidi, Y., Qallandar, O. B., Evenden, J., Alifui-Segbaya, F. & Ahmed, K. E. (2020). Accuracy of 3-Dimensionally Printed Full-Arch Dental Models: A Systematic Review. *J. Clin. Med.* *9*, 3357.
80. Lee, M. P. *et al.* (2015). Development of a 3D printer using scanning projection stereolithography. *Sci. Rep.* *5*, 9875.
81. He, Y., Wu, Y., Fu, J. Z., Gao, Q. & Qiu, J. J. (2016). Developments of 3D Printing Microfluidics and Applications in Chemistry and Biology: a Review. *Electroanalysis* *28*, 1658–1678.
82. Bagheri Saed, A. *et al.* (2020). Functionalized poly L-lactic acid synthesis and optimization of process parameters for 3D printing of porous scaffolds via digital light processing (DLP) method. *J. Manuf. Process.* *56*, 550–561.
83. Bernal, P. N. *et al.* (2019). Volumetric Bioprinting of Complex Living-Tissue Constructs within Seconds. *Adv. Mater.* *31*, 1904209.
84. Shusteff, M. *et al.* (2017). One-step volumetric additive manufacturing of complex polymer structures. *Sci. Adv.* *3*, eaao5496.
85. Loterie, D., Delrot, P. & Moser, C. (2020). High-resolution tomographic volumetric additive manufacturing. *Nat. Commun.* *11*, 852.
86. Nguyen, A. K. & Narayan, R. J. (2017). Two-photon polymerization for biological applications. *Mater. Today* *20*, 314–322.
87. Low, Z. X. *et al.* (2017). Perspective on 3D printing of separation membranes and comparison to related unconventional fabrication techniques. *J. Memb. Sci.* *523*, 596–613.
88. Yang, Q. *et al.* (2021). Recent progress of 3D-printed microneedles for transdermal drug delivery. *Int. J. Pharm.* *593*, 120106.
89. Tumbleston, J. R. *et al.* (2015). Continuous liquid interface production of 3D objects. *Science* (80-.). *347*, 1349–1352.
90. Bloomquist, C. J. *et al.* (2018). Controlling release from 3D printed medical devices using CLIP and drug-loaded liquid resins. *J. Control. Release* *278*, 9–23.
91. Nagarkar, R., Singh, M., Nguyen, H. X. & Jonnalagadda, S. (2020). A review of recent advances in microneedle technology for transdermal drug delivery. *J. Drug Deliv. Sci. Technol.* *59*, 101923.
92. Johnson, A. R. *et al.* (2016). Single-step fabrication of computationally designed microneedles by continuous liquid interface production. *PLoS One* *11*, e0162518.
93. Quan, H. *et al.* (2020). Photo-curing 3D printing technique and its challenges. *Bioact. Mater.* *5*, 110–115.
94. Caudill, C. L., Perry, J. L., Tian, S., Luft, J. C. & DeSimone, J. M. (2018). Spatially

- controlled coating of continuous liquid Interface production microneedles for transdermal protein delivery. *J. Control. Release* **284**, 122–132.
- 95. Doraiswamy, A. *et al.* (2006). Two photon induced polymerization of organic-inorganic hybrid biomaterials for microstructured medical devices. *Acta Biomater.* **2**, 267–275.
 - 96. Balmert, S. C. *et al.* (2020). Dissolving undercut microneedle arrays for multicomponent cutaneous vaccination. *J. Control. Release* **317**, 336–346.
 - 97. Rad, Z. F. *et al.* (2017). High-fidelity replication of thermoplastic microneedles with open microfluidic channels. *Microsystems Nanoeng.* **3**, 17034.
 - 98. Liao, C., Anderson, W., Antaw, F. & Trau, M. (2019). Two-Photon Nanolithography of Tailored Hollow three-dimensional Microdevices for Biosystems. *ACS Omega* **4**, 1401–1409.
 - 99. Trautmann, A., Roth, G. L., Nujiqi, B., Walther, T. & Hellmann, R. (2019). Towards a versatile point-of-care system combining femtosecond laser generated microfluidic channels and direct laser written microneedle arrays. *Microsystems Nanoeng.* **5**, 6.
 - 100. Gittard, S. D. *et al.* (2009). Fabrication of polymer microneedles using a two-photon polymerization and micromolding process. *J. Diabetes Sci. Technol.* **3**, 304–311.
 - 101. Gittard, S. D. *et al.* (2011). Multiphoton microscopy of transdermal quantum dot delivery using two photon polymerization-fabricated polymer microneedles. *Faraday Discuss.* **149**, 171–185.
 - 102. Nguyen, A. K. *et al.* (2019). Microneedle-Based Delivery of Amphotericin B for Treatment of Cutaneous Leishmaniasis. *Biomed. Microdevices* **21**, 8.
 - 103. Gittard, S. D. *et al.* (2010). Two photon polymerization-micromolding of polyethylene glycol-gentamicin sulfate microneedles. *Adv. Eng. Mater.* **12**, B77–B82.
 - 104. Cordeiro, A. S. *et al.* (2020). Two-Photon Polymerisation 3D Printing of Microneedle Array Templates with Versatile Designs: Application in the Development of Polymeric Drug Delivery Systems. *Pharm. Res.* **37**, 174.
 - 105. Battisti, M. *et al.* (2019). Non-invasive Production of Multi-Compartmental Biodegradable Polymer Microneedles for Controlled Intradermal Drug Release of Labile Molecules. *Front. Bioeng. Biotechnol.* **7**, 296.
 - 106. Moussi, K., Bukhamsin, A., Hidalgo, T. & Kosel, J. (2020). Biocompatible 3D Printed Microneedles for Transdermal, Intradermal, and Percutaneous Applications. *Adv. Eng. Mater.* **22**, 1901358.
 - 107. Szeto, B. *et al.* (2021). Novel 3D-printed hollow microneedles facilitate safe, reliable, and informative sampling of perilymph from guinea pigs. *Hear. Res.* **400**, 108141.
 - 108. Suzuki, M., Sawa, T., Takahashi, T. & Aoyagi, S. (2015). Fabrication of microneedle mimicking mosquito proboscis sing nanoscale 3D laser lithography system. *Int. J. Autom. Technol.* **9**, 655–661.
 - 109. Plamadeala, C. *et al.* (2020). Bio-inspired microneedle design for efficient drug/vaccine

coating. *Biomed. Microdevices* **22**, 8.

110. El-Tamer, A., Hinze, U. & Chichkov, B. N. (2020). Two-Photon Polymerization in Optics, Microfluidics, and Biomedicine. in *Handbook of Laser Micro- and Nano-Engineering* (ed. Sugioka, K.) 1–44 (Springer International Publishing, 2020). doi:10.1007/978-3-319-69537-2_35-1.
111. Huang, L. *et al.* (2017). Ultrafast Digital Printing toward 4D Shape Changing Materials. *Adv. Mater.* **29**, 1605390.
112. Khorsandi, D. *et al.* (2021). 3D and 4D printing in dentistry and maxillofacial surgery: Printing techniques, materials, and applications. *Acta Biomater.* **122**, 26–49.
113. Zhou, W. *et al.* (2020). 4D-Printed Dynamic Materials in Biomedical Applications: Chemistry, Challenges, and Their Future Perspectives in the Clinical Sector. *J. Med. Chem.* **63**, 8003–8024.
114. Zhang, Z., Demir, K. G. & Gu, G. X. (2019). Developments in 4D-printing: a review on current smart materials, technologies, and applications. *Int. J. Smart Nano Mater.* **10**, 205–224.
115. Chen, Z. *et al.* (2018). Additive Manufacturing of Honeybee-Inspired Microneedle for Easy Skin Insertion and Difficult Removal. *ACS Appl. Mater. Interfaces* **10**, 29338–29346.
116. Linh, V. T. N. *et al.* (2021). Bioinspired plasmonic nanoflower-decorated microneedle for label-free intradermal sensing. *Appl. Surf. Sci.* **551**, 149411.
117. Kim, Y. C., Quan, F. S., Compans, R. W., Kang, S. M. & Prausnitz, M. R. (2011). Stability kinetics of influenza vaccine coated onto microneedles during drying and storage. *Pharm. Res.* **28**, 135–144.
118. Saviola, A. J., Peichoto, M. E. & Mackessy, S. P. (2014). Rear-fanged snake venoms: An untapped source of novel compounds and potential drug leads. *Toxin Rev.* **33**, 185–201.
119. Young, B. A. *et al.* (2011). Tears of venom: Hydrodynamics of reptilian envenomation. *Phys. Rev. Lett.* **106**, 198103.
120. Hischen, F. *et al.* (2018). The external scent efferent system of selected European true bugs (Heteroptera): A biomimetic inspiration for passive, unidirectional fluid transport. *J. R. Soc. Interface* **15**, 20170975.
121. Mizuno, Y. *et al.* (2021). Fabrication of novel-shaped microneedles to overcome the disadvantages of solid microneedles for the transdermal delivery of insulin. *Biomed. Microdevices* **23**, 1–8.
122. Plamadeala, C. *et al.* (2018). Three-Dimensional Photonic Structures Fabricated by Two-Photon Polymerization for Microfluidics and Microneedles. *Int. Conf. Transparent Opt. Networks 2018-July*, 2018–2021.
123. Lifka, S., Hischen, F., Heitz, J. & Baumgartner, W. (2021). An Optimised Surface Structure for Passive, Unidirectional Fluid Transport Bioinspired by True Bugs. *J. Bionic Eng.* **18**, 375–386.

124. Ma, G. & Wu, C. (2017). Microneedle, bio-microneedle and bio-inspired microneedle: A review. *J. Control. Release* *251*, 11–23.
125. Zhang, F. *et al.* (2019). Mussel-inspired dopamine-CuII coatings for sustained in situ generation of nitric oxide for prevention of stent thrombosis and restenosis. *Biomaterials* *194*, 117–129.
126. Lee, H., Dellatore, S. M., Miller, W. M. & Messersmith, P. B. (2007). Mussel-inspired surface chemistry for multifunctional coatings. *Science* (80-.). *318*, 426–430.
127. Wang, R. *et al.* (2017). A Biomimetic Mussel-Inspired ϵ -Poly-l-lysine Hydrogel with Robust Tissue-Anchor and Anti-Infection Capacity. *Adv. Funct. Mater.* *27*,
128. Kim, D. W. *et al.* (2019). Highly Permeable Skin Patch with Conductive Hierarchical Architectures Inspired by Amphibians and Octopi for Omnidirectionally Enhanced Wet Adhesion. *Adv. Funct. Mater.* *29*, 1807614.
129. Baik, S. *et al.* (2017). A wet-tolerant adhesive patch inspired by protuberances in suction cups of octopi. *Nature* *546*, 396–400.
130. Liang, Y., He, J. & Guo, B. (2021). Functional Hydrogels as Wound Dressing to Enhance Wound Healing. *ACS Nano* *15*, 12687–12722.
131. Xu, Z., Han, S., Gu, Z. & Wu, J. (2020). Advances and Impact of Antioxidant Hydrogel in Chronic Wound Healing. *Adv. Healthc. Mater.* *9*, 1901502.
132. Kendall, M. A. F., Carter, F. V., Mitchell, T. J. & Bellhouse, B. J. (2001). Comparison of the transdermal ballistic delivery of micro-particles into human and porcine skin. in *Annual Reports of the Research Reactor Institute, Kyoto University* vol. 3 2991–2994 (2001).
133. Park, S. Y. *et al.* (2014). Wound healing potential of antibacterial microneedles loaded with green tea extracts. *Mater. Sci. Eng. C* *42*, 757–762.
134. Su, Y. *et al.* (2020). Dissolvable Microneedles Coupled with Nanofiber Dressings Eradicate Biofilms via Effectively Delivering a Database-Designed Antimicrobial Peptide. *ACS Nano* *14*, 11775–11786.
135. Zhang, X. *et al.* (2020). Black Phosphorus-Loaded Separable Microneedles as Responsive Oxygen Delivery Carriers for Wound Healing. *ACS Nano* *14*, 5901–5908.
136. Das, R. *et al.* (2018). Biomechanical Evaluation of Wasp and Honeybee Stingers. *Sci. Rep.* *8*, 1–13.
137. Ling, J. *et al.* (2016). Insertion and Pull Behavior of Worker Honeybee Stinger. *J. Bionic Eng.* *13*, 303–311.
138. Tran, L. G., Nguyen, T. Q. & Park, W. T. (2019). Bio-Inspired Barbed Microneedle for Skin Adhesion with Interlocking Mechanics. in *Proceedings of the IEEE International Conference on Micro Electro Mechanical Systems (MEMS)* vols 2019-Janua 547–550 (Institute of Electrical and Electronics Engineers Inc., 2019).
139. Guo, M., Wang, Y., Gao, B. & He, B. (2021). Shark Tooth-Inspired Microneedle Dressing for Intelligent Wound Management. *ACS Nano*.

140. Abolhassani, N., Patel, R. & Moallem, M. (2007). Needle insertion into soft tissue: A survey. *Med. Eng. Phys.* *29*, 413–431.
141. Halstuch, D. *et al.* (2018). Assessment of needle tip deflection during transrectal guided prostate biopsy: Implications for targeted biopsies. *J. Endourol.* *32*, 252–256.
142. Wu, J. S., Goldsmith, J. D., Horwich, P. J., Shetty, S. K. & Hochman, M. G. (2008). Bone and soft-tissue lesions: What factors affect diagnostic yield of image-guided core-needle biopsy? *Radiology* *248*, 962–970.
143. Li, A. D. R., Putra, K. B., Chen, L., Montgomery, J. S. & Shih, A. (2020). Mosquito proboscis-inspired needle insertion to reduce tissue deformation and organ displacement. *Sci. Rep.* *10*, 1–14.
144. Aoyagi, S., Izumi, H. & Fukuda, M. (2008). Biodegradable polymer needle with various tip angles and consideration on insertion mechanism of mosquito's proboscis. *Sensors Actuators, A Phys.* *143*, 20–28.
145. Yan, L., Alba, M., Tabassum, N. & Voelcker, N. H. (2019). Micro- and Nanosystems for Advanced Transdermal Delivery. *Adv. Ther.* *2*, 1900141.
146. Singh, P. *et al.* (2019). Polymeric microneedles for controlled transdermal drug delivery. *J. Control. Release* *315*, 97–113.
147. Mandal, A. *et al.* (2018). Cell and fluid sampling microneedle patches for monitoring skin-resident immunity. *Sci. Transl. Med.* *10*,
148. Donnelly, R. F. *et al.* (2014). Microneedle-mediated minimally invasive patient monitoring. *Ther. Drug Monit.* *36*, 10–17.
149. Muller, D. A., Corrie, S. R., Coffey, J., Young, P. R. & Kendall, M. A. (2012). Surface modified microprojection arrays for the selective extraction of the dengue virus NS1 protein as a marker for disease. *Anal. Chem.* *84*, 3262–3268.
150. Huang, Z. *et al.* (2018). A General Approach for Fluid Patterning and Application in Fabricating Microdevices. *Adv. Mater.* *30*, 1802172.
151. Xianyu, Y. *et al.* (2018). Controllable Assembly of Enzymes for Multiplexed Lab-on-a-Chip Bioassays with a Tunable Detection Range. *Angew. Chemie - Int. Ed.* *57*, 7503–7507.
152. Song, Y. *et al.* (2018). Interfacially Polymerized Particles with Heterostructured Nanopores for Glycopeptide Separation. *Adv. Mater.* *30*, 1803299.
153. Zhang, X., Chen, G., Bian, F., Cai, L. & Zhao, Y. (2019). Encoded Microneedle Arrays for Detection of Skin Interstitial Fluid Biomarkers. *Adv. Mater.* *31*, 1902825.
154. Wang, Z. *et al.* (2021). Microneedle patch for the ultrasensitive quantification of protein biomarkers in interstitial fluid. *Nat. Biomed. Eng.* *5*, 64–76.
155. Coffey, J. W., Meliga, S. C., Corrie, S. R. & Kendall, M. A. F. (2016). Dynamic application of microprojection arrays to skin induces circulating protein extravasation for enhanced biomarker capture and detection. *Biomaterials* *84*, 130–143.

156. Anker, J. N. *et al.* (2009). Biosensing with plasmonic nanosensors. *Nanosci. Technol. A Collect. Rev. from Nat. Journals* 308–319 doi:10.1142/9789814287005_0032.
157. Zhang, X., Fu, X., Chen, G., Wang, Y. & Zhao, Y. (2021). Versatile Ice Microneedles for Transdermal Delivery of Diverse Actives. *Adv. Sci.* 8, 2101210.
158. Barber, A. H., Lu, D. & Pugno, N. M. (2015). Extreme strength observed in limpet teeth. *J. R. Soc. Interface* 12, 20141326.
159. Kim, J. *et al.* (2018). Bioinspired microneedle insertion for deep and precise skin penetration with low force: Why the application of mechanophysical stimuli should be considered. *J. Mech. Behav. Biomed. Mater.* 78, 480–490.
160. Chen, G. *et al.* (2020). Transdermal cold atmospheric plasma-mediated immune checkpoint blockade therapy. *Proc. Natl. Acad. Sci. U. S. A.* 117, 3687–3692.
161. Carlotti, M. & Mattoli, V. (2019). Functional Materials for Two-Photon Polymerization in Microfabrication. *Small* 15, 1902687.
162. Ye, Y., Yu, J., Wen, D., Kahkoska, A. R. & Gu, Z. (2018). Polymeric microneedles for transdermal protein delivery. *Adv. Drug Deliv. Rev.* 127, 106–118.
163. Jiang, T. *et al.* (2020). Progress in transdermal drug delivery systems for cancer therapy. *Nano Res.* 13, 1810–1824.
164. Alimardani, V., Abolmaali, S. S., Tamaddon, A. M. & Ashfaq, M. (2021). Recent advances on microneedle arrays-mediated technology in cancer diagnosis and therapy. *Drug Deliv. Transl. Res.* 11, 788–816.
165. Zhi, D. *et al.* (2021). Microneedles for gene and drug delivery in skin cancer therapy. *J. Control. Release*.
166. Khan, S. *et al.* (2021). Diagnostic and drug release systems based on microneedle arrays in breast cancer therapy. *J. Control. Release*.
167. Yu, J., Zhang, Y., Yan, J., Kahkoska, A. R. & Gu, Z. (2018). Advances in bioresponsive closed-loop drug delivery systems. *Int. J. Pharm.* 544, 350–357.
168. Erdem, Ö., Es, I., Akceoglu, G. A., Saylan, Y. & Inci, F. (2021). Recent Advances in Microneedle-Based Sensors for Sampling, Diagnosis and Monitoring of Chronic Diseases. *Biosensors* 11, 296.
169. Than, A. *et al.* (2018). Self-implantable double-layered micro-drug-reservoirs for efficient and controlled ocular drug delivery. *Nat. Commun.* 9, 4433.
170. Xie, X. *et al.* (2017). Analgesic Microneedle Patch for Neuropathic Pain Therapy. *ACS Nano* 11, 395–406.
171. Tang, J. *et al.* (2018). Cardiac cell–integrated microneedle patch for treating myocardial infarction. *Sci. Adv.* 4, eaat9365.
172. Yang, G. *et al.* (2019). A Therapeutic Microneedle Patch Made from Hair-Derived Keratin for Promoting Hair Regrowth. *ACS Nano* 13, 4354–4360.

173. Than, A. *et al.* (2017). Transdermal Delivery of Anti-Obesity Compounds to Subcutaneous Adipose Tissue with Polymeric Microneedle Patches. *Small Methods* *1*, 1700269.
174. Zhang, Y. *et al.* (2017). Locally Induced Adipose Tissue Browning by Microneedle Patch for Obesity Treatment. *ACS Nano* *11*, 9223–9230.
175. Caffarel-Salvador, E. *et al.* (2021). A microneedle platform for buccal macromolecule delivery. *Sci. Adv.* *7*, eabe2620.
176. Zhang, X., Chen, G., Fu, X., Wang, Y. & Zhao, Y. (2021). Magneto-Responsive Microneedle Robots for Intestinal Macromolecule Delivery. *Adv. Mater.* *2104932*.